Research Square

Preprints are preliminary reports that have not undergone peer review.
They should not be considered conclusive, used to inform clinical practice,
or referenced by the media as validated information.

Biological and comparative genomic characterization of Staphylococcus aureus phage SJP49-2 and its effects on biofilm biomass

Qiang He
Xinjiang Agricultural University
Jian Qi
Xinjiang Agricultural University
Xue Han
Xinjiang Agricultural University
Bin Peng
pengbinwho@163.com

Xinjiang Agricultural University

Research Article

Keywords: Staphylococcus aureus, bacteriophage, comparative genomics, biofilm biomass, temperate potential

Posted Date: November 13th, 2026

DOI: https://doi.org/10.21203/rs.3.rs-11542015/v1

License: This work is licensed under a Creative Commons Attribution 4.0 International License.
Read Full License

Additional Declarations: No competing interests reported.

Biological and comparative genomic characterization of *Staphylococcus aureus* phage SJP49-2 and its effects on biofilm biomass

Qiang He[1,2], Jian Qi[1,2], Xue Han[1,2], Bin Peng[1,2*]

1 College of Veterinary Medicine, Xinjiang Agricultural University, Urumqi, China

2 Xinjiang Regional Key Laboratory of Clinical Veterinary Medicine Research, Xinjiang Agricultural University, Urumqi, China

First author: Qiang He; email: 2568852833@qq.com

* Correspondence: Bin Peng, pengbinwho@163.com

Postal address: College of Veterinary Medicine, Xinjiang Agricultural University, Urumqi, China

Abstract

Background: Biofilms complicate control of *Staphylococcus aureus* in food-related environments, and susceptibility to phages varies among strains. This study characterized phage SJP49-2 using morphology, lysis coverage across 92 laboratory-maintained strains, environmental stability, culture propagation, planktonic growth, biofilm biomass and a beef surface model. Host and phage genomes were analyzed, and SJP49-2 was compared with 19 reference phage genomes. Phenotypic assays were conducted as single experiments with technical replication and descriptive analysis.

Results: SJP49-2 showed lysis against 64 of 92 strains (69.57%). At the highest tested doses, crystal violet signals during biofilm formation and after treatment of established biofilms were 79.36% and 94.80% lower than their controls, respectively. In beef, the

inoculation scheme at a multiplicity of infection of 1000 had an 8 h bacterial count 2.08 $\log_{10}$ units below the control and a rise from its own baseline 0.45 $\log_{10}$ units smaller than the control; starting counts differed with the inoculation schemes. Sequencing generated 2,461,307 raw and 2,377,351 filtered read pairs. The 44,239 bp assembly contained no ambiguous bases, had a GC content of 35.38% and contained 69 GeneMarkS-predicted coding sequences with 93.13% nonoverlapping genomic coverage. Genomic annotations supported temperate potential; general protein-product discrepancies qualified the interpretation of negative database screens. The existing 20-genome comparison contained 383 gene clusters, including 11 strict core clusters.

Conclusions: SJP49-2 exhibited antibacterial and biofilm-biomass-reducing phenotypes under the tested conditions. The beef observations were consistent with growth limitation within the tested inoculation schemes. Its genomic features and candidate antibacterial proteins provide a basis for further investigation of phage–host interactions and food-related biocontrol.

Keywords: *Staphylococcus aureus*; bacteriophage; comparative genomics; biofilm biomass; temperate potential

Background

Staphylococcus aureus is a foodborne pathogen of concern in meat, dairy products, and other foods. Its food safety impact arises from both viable-cell contamination and the production of enterotoxins as toxigenic strains multiply in food. Consumption of food containing preformed enterotoxins can cause staphylococcal food poisoning. In an investigation of a large dairy-associated outbreak in Japan, Asao et al. reported that heat treatment killed the contaminating *S. aureus*, whereas enterotoxin A retained sufficient biological activity to cause illness [1]. Control strategies must therefore limit contamination

and bacterial growth during processing and storage. Eliminating viable cells at the end of processing does not necessarily eliminate enterotoxins already present.

S. aureus contamination in meat also involves antimicrobial resistance and persistence in processing environments. Waters et al. detected *S. aureus* in 47% of 136 retail meat and poultry samples in the United States; 52% of the isolates exhibited intermediate susceptibility or resistance to at least three antimicrobial classes [2]. These findings support considering bacterial loads, strain backgrounds, and resistance characteristics together when assessing meat contamination. *S. aureus* can also adhere to food-contact surfaces and form biofilms. Using a meat-based culture system, de Souza et al. demonstrated biofilm formation by food-processing isolates on stainless steel and polypropylene, with attached cells persisting under the tested temperature conditions [3]. Food-related antimicrobial strategies should consequently address both planktonic cells and surface-associated populations.

Cleaning and disinfection help interrupt surface contamination, but mature biofilms complicate complete cell removal. In the meat-based system described above, neither 250 mg/L sodium hypochlorite nor 30 mg/L peracetic acid completely removed attached *S. aureus* from the tested surfaces [3]. Disinfection performance thus depends on the attachment state and treatment conditions, and findings obtained with planktonic cells cannot be directly extrapolated to biofilms. Evaluating inhibition of biofilm formation and treatment of established biofilms separately, followed by assessment in a food matrix, provides a more complete basis for developing *S. aureus* control strategies.

Bacteriophages exert antibacterial effects by recognizing susceptible hosts and establishing infection, providing a biological approach to targeted *S. aureus* control. Recent studies have combined phage characterization with evaluations of planktonic cells, biofilms, and meat models. Ma et al. reported that phage SPB inhibited planktonic methicillin-resistant *S. aureus* and showed activity against both biofilm formation and established biofilms [4].

Gungor et al. evaluated slaughterhouse-derived phages and their combinations against biofilm-forming, multidrug-resistant *S. aureus* in a beef model [5]. These studies provide an experimental basis for food-related phage research and demonstrate the value of assessing host susceptibility, antibiofilm activity, and performance in food matrices together.

The activity spectrum and development pathway of a phage also depend on the genetic characteristics of both the phage and its host. A study of 259 *S. aureus* strains and eight phages by Moller et al. identified strain-dependent differences in susceptibility and experimentally established the contributions of several host genes to infection phenotypes [6]. A positive lysis phenotype and efficiency of plating (EOP) describe different aspects of susceptibility and productive infection and should be distinguished during phage screening [7]. Comparative genomic studies have also shown that staphylococcal phages with similar genome lengths can differ in gene content and functional modules [8, 9]. Lifestyle-associated genes and screening for known risk-associated genes provide additional evidence relevant to infection mechanisms and suitability for application. The endolysin and tail hydrolase of temperate phage DW2 have demonstrated antibacterial activity, illustrating distinct research and development opportunities for intact phages and phage-derived proteins [10]. Integrating antibacterial phenotypes with the genomes of both partners can therefore help define a candidate phage's research value and subsequent development priorities.

This study investigated *S. aureus* phage SJP49-2 and its host, strain P49-2, through antibacterial evaluations of planktonic growth, biofilms, and a beef surface model. Plaque observations and transmission electron microscopy were combined with assessments of lysis coverage, propagation dynamics in the culture system, and infectivity after temperature and pH treatments. Inhibition of biofilm formation and reduction of attached biomass in established biofilms were evaluated separately, and bacterial counts were compared among beef inoculation schemes. Host and phage genome characterization, lifestyle-associated gene

evidence, and comparisons with 19 reference phages were then used to relate the antibacterial phenotype of SJP49-2 to its genomic characteristics. These analyses provide a basis for studies of infection mechanisms, antimicrobial components, and food-related experimental models.

Methods

Bacterial Strains and Phages

All 92 *S. aureus* strains used in this study were maintained in the laboratory collection. Strain P49-2 served as the host for phage propagation and phenotypic assays. Phages SJP49-2, PS9-1, PS15-2, and PS35-1 were isolated previously from wastewater from the same slaughterhouse. Their lysis coverage was compared against this collection, and SJP49-2 was selected for subsequent characterization because it showed the highest observed coverage. The collection and strain identifiers are represented in Figure S1; the reported coverage describes this tested collection.

Plaque Observation and Transmission Electron Microscopy

Plaque appearance on the host bacterial lawn was observed and photographed to record morphology and distribution. Phage suspensions were submitted to Wuhan Servicebio Technology Co., Ltd. (Wuhan, China) for sample preparation and transmission electron microscopy. Images were acquired using a Hitachi transmission electron microscope at an accelerating voltage of 80 kV, as recorded in the original images. The two virion distribution fields were acquired at 50,000× magnification, and the head-focused field at 120,000×, with original scale bars of 200 and 100 nm, respectively. Head outlines and tail configurations were assessed qualitatively. The plaque image was selected from an original area without the handwritten experimental label; the original TEM images and scale bars were retained.

Lysis Coverage and Phage Titer Determination

Lysis coverage was evaluated against the 92 laboratory-maintained *S. aureus* strains. Coverage was calculated as the number of strains showing the recorded lysis phenotype divided by 92, multiplied by 100%. Individual strain responses were retained in Figure S1. In accordance with the distinction between lysis screening and efficiency of plating described by Khan Mirzaei and Nilsson [7], these observations were reported as lysis coverage rather than assumed to demonstrate equivalent productive infection on every strain.

Titers were determined with reference to the double-agar overlay plaque assay [11]. Phage samples were serially diluted and assayed using P49-2 as the indicator strain. Titers were calculated as $T = \frac{N}{V \times d}$, where T is the titer (PFU/mL), N is the plaque count, V is the volume of diluted sample added (mL), and d is the dilution fraction. Titers from technical replicate plates within the same experiment were calculated individually before summarization.

Endpoint Titers at Different MOIs and Environmental Stability

Multiplicity of infection (MOI) was calculated as the ratio of infectious phages to viable host cells added to the culture: $MOI = \frac{C_p \times V_p}{C_b \times V_b}$, where C_p and C_b denote the phage titer and bacterial concentration, and V_p and V_b denote their respective added volumes. Initial MOIs of 1000, 100, 10, 1, 0.1, 0.01, 0.001, and 0.0001 were compared. Endpoint titers were measured after 4 h of phage–host coculture, with the incubation duration based on the approach of Ma et al. [4].

Temperature treatments were conducted at 4, 25 (room temperature), 37, 40, 50, 60, 70, and 80 °C; pH treatments covered pH 1–13. Each treatment lasted 1 h. Residual titers were

measured to compare infectivity after the temperature and pH treatments, following the evaluation framework in reference [4].

Results were expressed as PFU/mL and $\log_{10}$-transformed titers. Between-group log differences were calculated as $log_{10}(T_{reference}) - log_{10}(T_{treatment})$. The 25 °C group was the reference for temperature comparisons; pH comparisons used the residual titers after treatment.

Phage Propagation Kinetics

Phage titers were recorded every 10 min from 0 to 130 min and expressed as $\log_{10}$(PFU/mL). The time series described the rise in culture titer, the highest measured titer and subsequent changes. These operational propagation endpoints were distinguished from latent period and burst size as defined by Hyman and Abedon [12].

Host and Phage Genome Sequencing and Analysis

Library Preparation and Genome Assembly

Genome sequencing of host strain P49-2 and phage SJP49-2 was performed by Shanghai Personal Biotechnology Co., Ltd. Phage DNA was quantified using the Quant-iT PicoGreen dsDNA Assay Kit, and DNA integrity was assessed by 1% agarose gel electrophoresis. DNA was fragmented using Covaris, and libraries were prepared using the Illumina TruSeq Nano DNA LT workflow, including end repair, A-tailing, indexed adapter ligation, magnetic-bead purification and PCR enrichment. Library concentration and fragment size were assessed, with size analysis performed using an Agilent Bioanalyzer 2100. Libraries with an approximate insert size of 400 bp were sequenced on the Illumina NovaSeq platform in paired-end 2 × 250 bp mode. The host genome was sequenced in paired-end 2 × 150 bp mode.

Phage reads were processed using fastp v0.20.0 [13] to remove adapters and filter reads using a 50-bp length threshold and a mean quality threshold of 20; read pairs containing at least five ambiguous bases were excluded. Filtered reads were assembled de novo using SPAdes v3.12.0 [14], followed by sequence screening against the NCBI nucleotide (NT) database and polishing using Pilon v1.18 [15]. Host reads were processed using fastp v0.23.1 and assembled using SPAdes v3.15.4. Host scaffolds longer than 500 bp with a mean depth greater than 10 were retained. Read counts and nucleotide totals were calculated from the FASTQ files. The phage and host assemblies are available under GenBank accession QB220577 and WGS accession JCFQZX010000000, respectively. Sequencing and assembly characteristics are summarized in Additional file 1, Table S1; per-file FASTQ statistics are provided in Additional file 2.

Host Genome Identification and Functional Analysis

Host assembly completeness was assessed using CheckM [16], and taxonomic identification combined NCBI NT alignment with the GTDB-Tk classify_wf workflow [17]. Coding genes were predicted using GeneMarkS [18] and annotated against the nonredundant protein (NR), eggNOG and Swiss-Prot databases, the Kyoto Encyclopedia of Genes and Genomes (KEGG), and Gene Ontology (GO); eggNOG annotation used eggnog-mapper. tRNAs and rRNAs were predicted using tRNAscan-SE and Barrnap, respectively, and other noncoding RNAs were identified by Rfam alignment. Candidate CRISPR loci and prophage regions were predicted using CRISPRCasFinder and PhiSpy, respectively.

Host virulence-related sequences were aligned against the Set B virulence factor reference sequences using BLAST, with an E-value threshold of 1×10^{-5}, amino acid identity >60%, and alignment coverage ≥70% of the reference protein length. Comprehensive Antibiotic Resistance Database (CARD) homology searches used an E-value threshold of 1 ×

10^{-5}, identity >45%, and alignment coverage ≥70%, retaining the best hit. ResFinder was used for complementary analysis. Annotation entries were counted separately for virulence-related functional categories and CARD resistance mechanism categories.

Phage Gene Prediction and Functional Annotation

Phage coding sequences were predicted using GeneMarkS v4.32 [18], and noncoding RNAs were screened using Rfam v14.1 [19]. Predicted proteins were searched against NR and Swiss-Prot using DIAMOND v0.8.36 in blastp mode [20], with an E-value threshold of 1×10^{-6} and retention of the best hit. For eggNOG assignment, DIAMOND blastp searches required $E < 1 \times 10^{-6}$, identity >30% and alignment coverage of at least 70% of either protein. This annotation set was analyzed separately from the PhageScope eggNOG-mapper results. GO assignments were obtained using InterProScan v5.28-67.0 and InterPro2GO and summarized using map2slim v0.14 with the generic GO-slim set [21, 22]. KEGG annotation used KAAS v2.1 with the bidirectional best-hit strategy [23]. Software and analysis settings are summarized in Table S4. A machine-readable summary is provided in Additional file 3. Database-annotated CDS counts and overlapping GO/KEGG category entries were summarized separately; the latter describe annotations rather than expression or statistical enrichment. Figure 6 retains the PhageScope feature coordinates and product-based display groups, whereas Figure 7 summarizes the GeneMarkS set. GC content [(G + C)/(A + T + G + C)] and GC skew [(G - C)/(G + C)] were calculated for the existing genome display in 500-bp windows at 100-bp steps, with truncated terminal windows. Generic database terms and uncertain functions were not assigned experimentally established activities.

Base composition and ambiguous positions were calculated directly from the assembled FASTA sequence. Coding coverage was calculated as the union of GeneMarkS CDS intervals in the General Feature Format version 3 (GFF3) file, counting each genomic

position once. The summed CDS-length/genome-length ratio was calculated separately. GeneMarkS and PhageScope predictions were matched only when their start, end and strand agreed, and both identifiers were retained. Protein query coverage was calculated as the aligned query span divided by query length. Gene-level annotation evidence and coordinate cross-references are provided in Additional file 4.

Phage Lifestyle Prediction and Screening for Safety-Associated Genes

PhageScope [24] was used to predict lifestyle, annotate proteins and screen for virulence-factor and antimicrobial-resistance genes in the 44,239 bp SJP49-2 assembly, using the Virulence Factor Database (VFDB) and CARD as the respective reference resources. Candidate recombinase, repressor and antirepressor annotations were assessed by genomic coordinate, strand, protein length and annotation source and compared with NR, Swiss-Prot, eggNOG and KEGG results. Lifestyle-associated evidence is summarized in Table S3. Sequence-based functional assignments and database screening results were interpreted according to phage annotation and virulence-gene evidence [25, 26].

Reference Phage Collection and Comparative Genomics

Nineteen complete phage genomes with *S. aureus* recorded as the host and genomic homology to SJP49-2 were obtained from NCBI GenBank. Each reference consisted of a single assembled nucleotide sequence. Sequences containing ambiguous bases and exact duplicates were excluded. Phage names, accession numbers, countries or regions of origin, genome lengths, and GC contents were recorded. Reference sequences were downloaded on October 7, 2026; GC content was calculated as the proportion of G and C bases in each sequence. The references and SJP49-2 (sequencing sample SJP49_2) were annotated consistently using Prokka [27]. GFF files containing the genomic nucleotide sequences were

analyzed using Roary to identify homologous gene clusters [28]. Clusters were classified by prevalence across the 20 genomes as core (99%–100%), soft-core (95%–<99%), shell (15%–<95%), or cloud (<15%), corresponding here to presence in 20, 19, 3–18, or 1–2 genomes, respectively. A gene presence–absence matrix and comparative tree were used to display shared and variable gene content. A circular layout integrating the comparative tree and multiple metadata tracks was used to display sample relationships and genome features [29]. Tree topology and sample order were retained, and terminal tips were aligned to a common radius. From inner to outer, the tracks represented country of origin, genome length, and GC content. Genome length and GC content used consistent continuous color scales, and country used categorical colors. Samples without explicit country information were labeled Unspecified. The circular display represents clustering topology; branch lengths do not indicate evolutionary distances. The complete gene presence–absence matrix is shown in Figure 9.

For an independently reproducible sequence comparison, the SJP49-2 assembly was queried against the 19 reference FASTA sequences using local BLASTn v2.13.0+ [30] with task blastn, E-value 1 x 10^{-10}, up to 50 target sequences and up to 100 high-scoring segment pairs (HSPs) per target. Other settings were unchanged. Query and subject coverage were calculated as the union of their aligned nucleotide intervals across all reported HSPs, divided by the corresponding genome length. Identity and aligned length of the highest-bit-score HSP were reported separately. These summaries were not treated as average nucleotide identity (ANI) or whole-genome intergenomic similarity. Comparison summaries are provided in Additional file 5. The BLASTn command, HSP table, input sequences and scripts are provided in Additional file 6.

Assessment of Planktonic Host Growth

SJP49-2 and P49-2 were cocultured at MOIs of 1000, 100, 10, 1, and 0.1, with a control group included. Coculture initiation was defined as 0 min. Optical density at 600 nm (OD_{600}) was measured every 10 min through 300 min to assess host growth from changes in culture turbidity. This monitoring interval is consistent with the dynamic OD_{600} measurements used by Workman et al. in *S. aureus*–phage liquid growth assays [31].

Changes relative to each group's 0 min value were calculated as $\Delta OD_{600}(t) = OD_{600}(t) - OD_{600}(0)$. Measured and baseline-adjusted curves were displayed side by side to describe culture turbidity and its increase over time.

Endpoint OD_{600} and ΔOD_{600} were used to compare growth among treatments, and the time series were analyzed descriptively.

Assessment of Biofilm Formation and Established Biofilms

Biofilm formation and established-biofilm biomass were assessed using crystal violet staining, following the framework described by O'Toole and Haney et al. [32, 33] and the *S. aureus* phage method of Ma et al. [4], with the treatment groups specified below. In the formation assay, P49-2 was incubated with SJP49-2 at MOIs of 1000, 100, 10 and 1 at 37 °C for 24 h, alongside a phage-free control, with five technical replicate readings per group. For established biofilms, P49-2 was first incubated at 37 °C for 24 h, after which the biofilms were treated with SJP49-2 at 10^8, 10^7, 10^6 or 10^5 PFU/mL for 18 h. A phage-free control was included, with four technical replicate readings per group.

After incubation, nonadherent material was removed by washing. Attached biomass was stained with 1% crystal violet for 30 min, washed to remove excess stain, and the retained dye was dissolved in anhydrous ethanol. Absorbance was measured at 600 nm [4]. Crystal violet retention was used to quantify attached biomass [32, 33]. Absorbance values were

analyzed without blank subtraction, and percentage decreases were calculated relative to the corresponding phage-free controls.

Formation assay results were summarized as the mean ± standard deviation (SD) of the five technical replicate readings within the same experiment. SD described variation among wells. The percentage decrease in crystal violet signal relative to the control was calculated as $R = [1 - \frac{meanA_{treatment}}{meanA_{control}}] \times 100\%$, using absorbance values without blank subtraction.

Beef Surface Model

Sterile beef cubes measuring 2 × 2 × 2 cm were used as an inoculated food-matrix model; the recorded background count before inoculation was zero. Initial MOIs of 1000, 100 and 10 were established by adjusting the phage and bacterial input amounts, with a phage-free control included. Initial MOI denoted the ratio of input infectious phages to viable host cells [34]. As a consequence of the selected inoculation schemes, measured starting bacterial counts differed among groups. The inoculated beef cubes were incubated at 37 °C. At 0, 2, 4, 6 and 8 h, beef samples were ground and filtered, and the volume of filtrate recovered for bacterial enumeration was 1 mL per sample. The recovered filtrate was diluted and spread-plated on agar medium. Viable bacterial concentrations were calculated from colony counts, accounting for the dilution and plated volume, and expressed as CFU/mL of the recovered filtrate [35]. Each group's measured 0 h count was retained as its own baseline, so endpoint differences and changes during incubation could be described separately. The use of a beef matrix addresses the food-associated evaluation setting examined in previous *S. aureus* phage research [5].

Bacterial counts were $\log_{10}$-transformed for time-series plots. The increase relative to each group's 0 h count was calculated as $G(t) = log_{10}[\frac{N(t)}{N(0)}]$, where N(t) and N(0) denote that

group's count at time t and 0 h, respectively. This measure described relative growth under each inoculation scheme during the observation period.

The concurrent between-group count difference was calculated as $D(t) = log_{10}[N_{control}(t)] - log_{10}[N_{treatment}(t)]$. The difference in increases relative to each group's own baseline was calculated as $D_G(t) = G_{control}(t) - G_{treatment}(t)$, equivalent to D(t) − D(0). The former describes differences in counts at the same time point, whereas the latter describes differences in increases from baseline. Both measures were used for descriptive comparisons of the initial inoculation schemes.

Data Processing and Statistical Reporting

Each phenotypic assay was conducted as a single experiment with technical replication within groups; no independent experimental batches were performed. Biofilm formation was summarized from five technical replicate readings per group as the mean ± standard deviation (SD), using n − 1 in the SD denominator. Established-biofilm results were summarized from four technical replicate readings per group, with individual readings displayed. Here, n denotes within-experiment readings rather than independent experimental batches, consistent with the distinction between observational units and independently replicated experiments [36].

Data were analyzed descriptively using observed values, means, within-experiment SDs, concurrent between-group differences and changes relative to each group's starting value. Reporting followed the SAMPL guidelines [37]. Technical replicates and repeated time points were not counted as independent experimental batches, and no inferential P values were reported. Where only aggregate values were available, no replicate-level SD was reconstructed.

Computational and writing assistance

A large language model (OpenAI Codex) assisted with language editing, literature-supported interpretation and drafting of analysis scripts. Quantitative sequencing additions were obtained by running documented scripts on the delivered FASTQ, FASTA, GFF3 and annotation tables; the tool was not used as a source of experimental observations.

Results

Morphology and Lysis Coverage of Phage SJP49-2

Plaque and Virion Morphology

SJP49-2 produced pinpoint plaques on the host bacterial lawn. Most plaques were approximately circular, with numerous dispersed plaques visible across the photographed area and some closely spaced neighboring plaques (Figure 1a). Transmission electron microscopy revealed head–tail virions in both lower-magnification fields. The heads had approximately isometric, polyhedral outlines, and the tails were long, slender, and flexible, without an evident contractile sheath (Figure 1b,c). The higher-magnification image further resolved the head outline (Figure 1d). These features are consistent with a siphovirus morphotype.

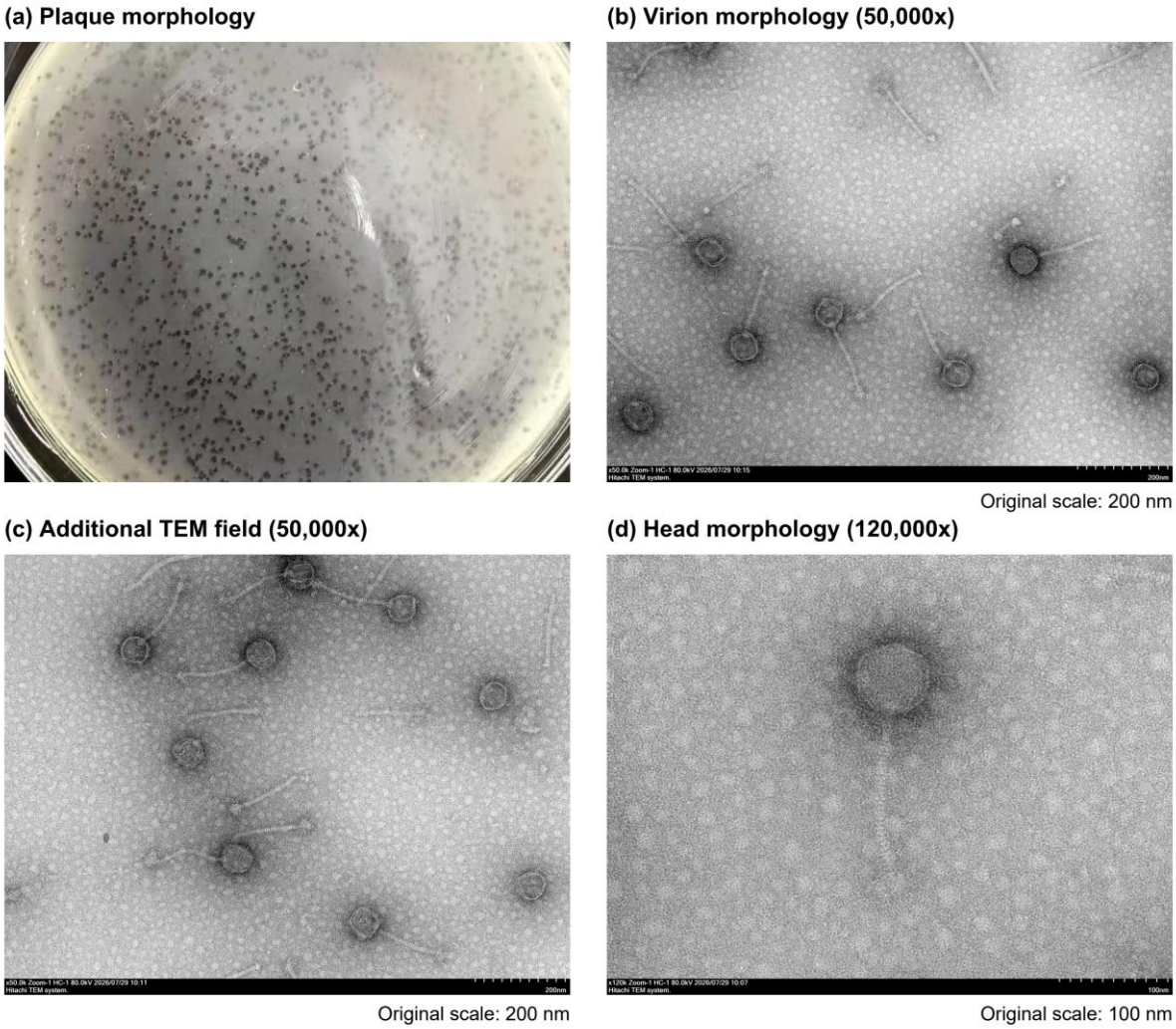


Figure 1. Plaque and virion morphology of phage SJP49-2.

(a) Representative pinpoint, predominantly circular plaques formed by SJP49-2 on a lawn of *Staphylococcus aureus* P49-2. The image was cropped from the original photograph to exclude the handwritten recording label. (b,c) TEM fields showing approximately isometric, polyhedral heads and long, slender, flexible tails; magnification, 50,000×; scale bars, 200 nm. (d) Higher-magnification TEM image showing the polyhedral head outline; magnification, 120,000×; scale bar, 100 nm. All TEM images were acquired at an accelerating voltage of 80 kV. Original TEM images and scale bars are retained.

Lysis Coverage among the Tested Strains

Among the 92 *S. aureus* strains tested, SJP49-2 lysed 64, corresponding to a lysis rate of 69.57%. PS9-1, PS15-2, and PS35-1 lysed 46, 45, and 38 strains, respectively, corresponding to rates of 50.00%, 48.91%, and 41.30%. SJP49-2 had the highest lysis coverage of the four candidates and was selected for subsequent characterization and application-oriented evaluation (Figure 2). Individual strain lysis profiles are shown in Figure S1.

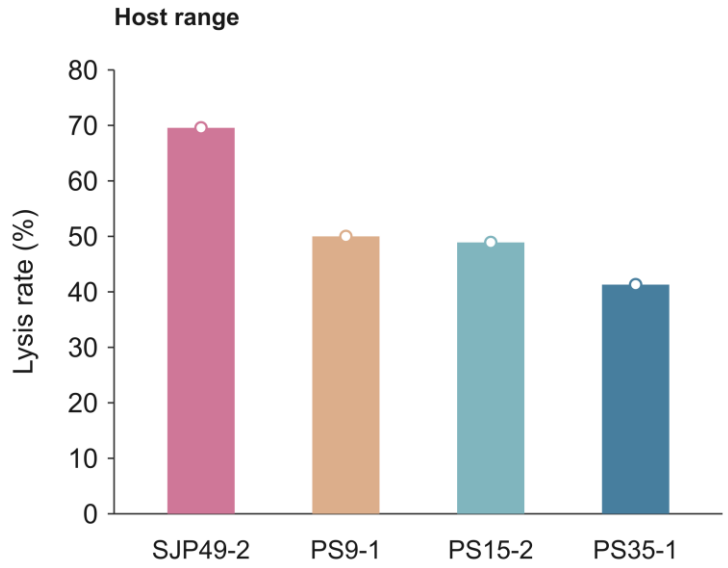


Figure 2. Lysis coverage of four candidate phages across 92 *Staphylococcus aureus* strains.

Bars and open circles show lysis coverage for each phage. SJP49-2, PS9-1, PS15-2, and PS35-1 lysed 64, 46, 45, and 38 strains, respectively, out of 92 strains tested for each phage.

Endpoint Titers of SJP49-2 at Different MOIs

Within the tested range, the endpoint titer of SJP49-2 varied with the initial MOI. The highest recorded value was 8.75×10^8 PFU/mL at an MOI of 100, followed by 5.82×10^8 PFU/mL at an MOI of 10. Titers at MOIs of 1000 and 1 were 2.95×10^8 and 2.96×10^8

PFU/mL, respectively. As the MOI decreased from 0.1 to 0.0001, the endpoint titer decreased from 1.18×10^8 to 1.53×10^6 PFU/mL (Figure 3a).

Under the tested conditions, an MOI of 100 yielded the highest endpoint titer and provides a starting condition for optimizing high-titer phage preparation.

Residual Titers after Temperature and pH Treatments

After 1 h of treatment, titers were 4.07×10^9 PFU/mL at 25 °C and 3.14×10^9 PFU/mL at 37 °C; the corresponding values at 4 and 40 °C were 6.63×10^8 and 5.87×10^8 PFU/mL. Titers at 50, 60, 70, and 80 °C were 4.70×10^5, 3.20×10^4, 6.80×10^3, and 8.10×10^2 PFU/mL, respectively. Compared with the 25 °C group, titers at 60, 70, and 80 °C were lower by 5.10, 5.78, and 6.70 $\log_{10}$ units, respectively, indicating substantially lower residual titers after high-temperature treatment. Residual infectious phages remained detectable after treatment at 80 °C (Figure 3b).

After 1 h of pH treatment, titers at pH 3, 4, and 5 were 1.58×10^6, 1.86×10^7, and 2.51×10^7 PFU/mL, respectively. Titers at pH 6, 7, and 8 were 4.27×10^8, 4.57×10^8, and 5.25×10^8 PFU/mL. Values at pH 9–11 were 3.55×10^7, 3.24×10^7, and 1.70×10^7 PFU/mL, respectively. Infectious phages were not detected at pH 1, 2, 12, or 13 (Figure 3c).

Residual titers at pH 6–8 were within the same order of magnitude, with a maximum difference of approximately 0.09 $\log_{10}$ units. Conditions near neutral pH therefore favored maintenance of SJP49-2 infectivity during the 1 h treatment.

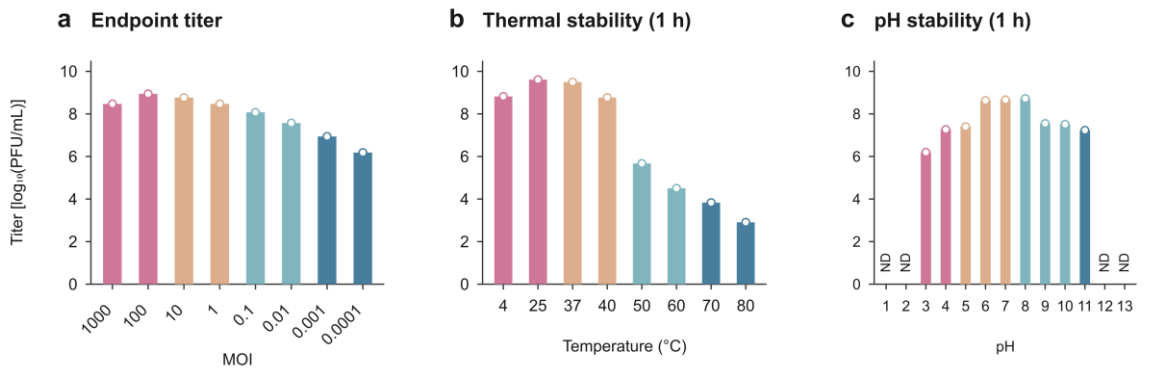


Figure 3. Endpoint titers and environmental stability of phage SJP49-2.

(a) Endpoint titers at different multiplicities of infection (MOIs). (b) Residual titers after 1 h at the indicated temperatures. (c) Residual titers after 1 h at the indicated pH values. Bars and open circles represent $\log_{10}$-transformed titers. ND, not detected.

Propagation Kinetics of SJP49-2

The SJP49-2 titer increased during the observation period and declined after reaching a peak. At 0 min, the titer was 5.50×10^3 PFU/mL; values at 10 and 20 min were 4.27×10^4 and 5.37×10^5 PFU/mL, respectively, increasing to 1.78×10^6 PFU/mL at 40 min. The titer reached 1.95×10^7 PFU/mL at 50 min, decreased slightly to 1.51×10^7 PFU/mL at 60 min, and then rose to 5.62×10^8 PFU/mL at 70 min. The highest value, 9.77×10^8 PFU/mL, occurred at 80 min. From 90 to 130 min, the titer gradually decreased from 6.45×10^8 to 2.95×10^8 PFU/mL (Figure 4).

The rapid increase occurred between 60 and 80 min, when the titer rose from 1.51×10^7 to 9.77×10^8 PFU/mL, a 64.70-fold increase equivalent to 1.81 $\log_{10}$ units. Together with the subsequent decline, this interval describes the rapid accumulation of phage titer and attainment of the peak in the culture system used.

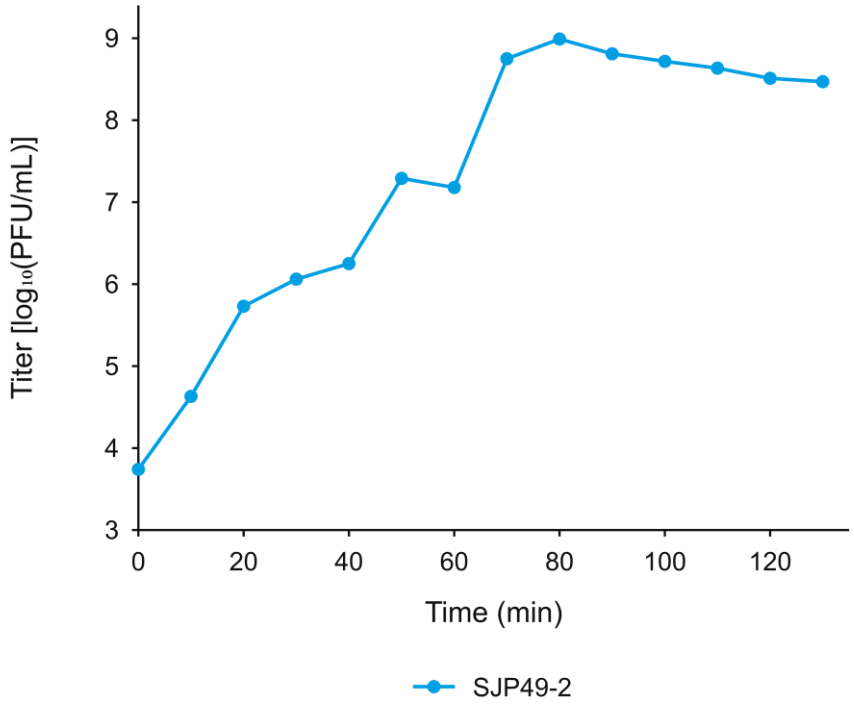


Figure 4. Propagation kinetics of phage SJP49-2.

Titers measured from 0 to 130 min are expressed as $\log_{10}$(PFU/mL). The highest measured titer occurred at 80 min. Lines connect successive sampling points.

Host and Phage Genome Analyses

Draft Genome Characteristics of Host Strain P49-2

Sequencing of host strain P49-2 yielded 7,818,262 raw reads, with Q20 and Q30 values of 99.25% and 96.54%, respectively. Quality filtering retained 7,625,172 reads comprising 1,144,829,689 bp of high-quality data, with a sequencing depth of 420×. The assembly totaled 2,720,755 bp, had a GC content of 32.71%, and contained 14 contigs and 10 scaffolds. The contig and scaffold N50 values were 314,291 and 614,552 bp, respectively; the longest scaffold was 1,027,301 bp. CheckM estimated completeness at 99.51%, and NT alignment and GTDB classification supported identification as *S. aureus*. A total of 2,518 open reading frames (ORFs) were predicted, with a combined coding length of 2,275,299 bp,

a coding proportion of 83.63%, and a mean ORF length of 903.61 bp. The host genome is associated with WGS accession JCFQZX000000000 (version JCFQZX010000000). The principal sequencing and assembly metrics for both samples are presented in Table S1.

Virulence and Resistance Annotations in Host Strain P49-2

Host virulence-related annotations included nutritional and metabolic factors, immune modulation, exotoxins, adherence, exoenzymes, effector delivery, stress survival, biofilm, and regulation categories (Figure 5a). Nutritional and metabolic factors had the highest count, with 29 entries; immune modulation and exotoxins each had 25, adherence had 19, exoenzymes had 18, and biofilm-associated annotations had four. CARD annotations included 32 entries for antibiotic target alteration, 16 for antibiotic efflux, and one each for target protection and target replacement (Figure 5b). ResFinder detected no positive hits. These homology-based annotations describe the host's virulence- and resistance-associated genetic background.

Host genome analysis identified five candidate CRISPR records, each containing one spacer, and candidate prophage regions designated pp1–pp5. These findings provide leads for investigating host defenses and phage-associated genetic elements.

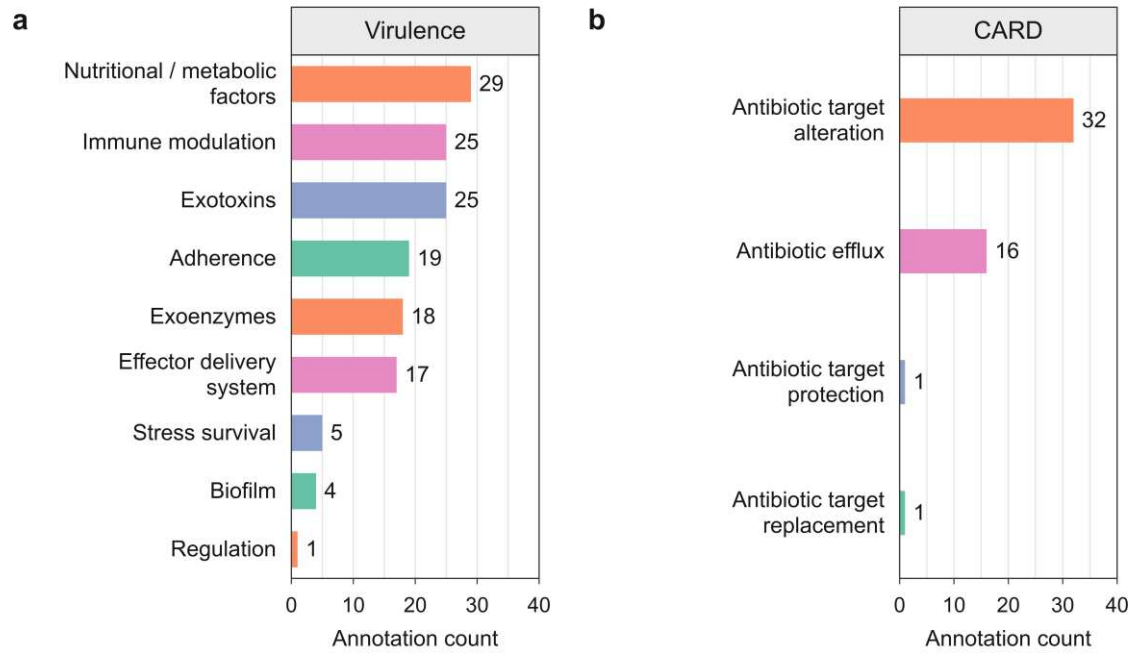


Figure 5. Virulence and antimicrobial resistance annotation categories in host strain P49-2.

(a) Virulence-related functional categories. (b) Antimicrobial resistance mechanisms annotated using CARD. Bars indicate the number of homologous annotation entries assigned to each category.

Genome Characteristics of Phage SJP49-2

Sequencing generated 4,922,614 raw reads (2,461,307 pairs), totaling 1,202,676,533 bases, with Q20 and Q30 values of 96.55% and 91.21%, respectively. Filtering retained 4,754,702 reads (2,377,351 pairs; 96.59%), totaling 1,125,702,666 bases (93.60%), with Q20 and Q30 values of 98.01% and 93.34%. The assembly comprised a single 44,239 bp sequence with no ambiguous bases and a GC content of 35.38% (GenBank accession QB220577). GeneMarkS predicted 69 CDSs with a summed length of 41,442 bp, a mean length of 600.61 bp and a maximum length of 2,871 bp. The summed CDS-length/genome-length ratio was 93.68%. After merging overlapping CDS intervals, the uniquely covered sequence totaled 41,198 bp (93.13%), leaving 3,041 bp outside predicted CDSs. Rfam screening detected no

noncoding RNA annotations. Sequencing and assembly metrics are provided in Table S1 and Additional file 2; the genome map in Figure 6 uses the PhageScope gene predictions.

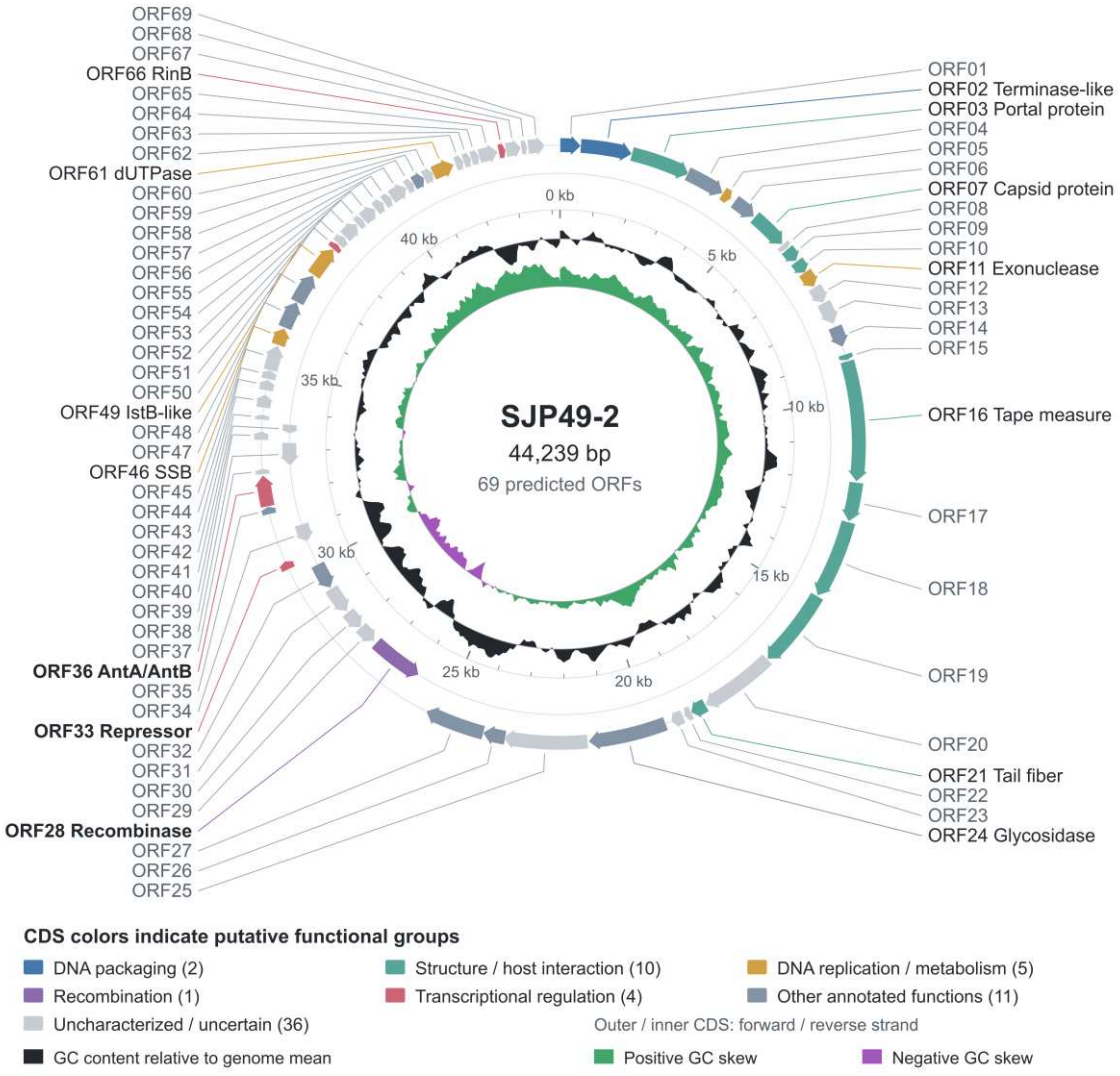


Figure 6. Annotated genome map of phage SJP49-2.

ORF01-ORF69 correspond to the PhageScope identifiers SJP49_2_1-SJP49_2_69. Colors indicate putative functions; inner rings show coordinates, GC content and GC skew. PhageScope and GeneMarkS predictions each contain 69 CDSs but have 58 exact coordinate-and-strand matches; their numbering is not universally interchangeable. GeneMarkS-to-PhageScope correspondence is recorded in Additional file 4. Circular display does not establish physical genome topology.

Functional Annotation of Phage SJP49-2

Of the 69 predicted ORFs, NR, GO, Swiss-Prot, KEGG, and eggNOG annotated 59, 14, 11, 5, and 3, respectively (85.51%, 20.29%, 15.94%, 7.25%, and 4.35%; Figure 7a). GO assignments comprised DNA binding (8 entries), cellular nitrogen compound metabolic process (5), biosynthetic process (2), hydrolase activity acting on carbon–nitrogen bonds (2), ion binding (2), catabolic process (1), and the molecular function parent term (2) (Figure 7b).

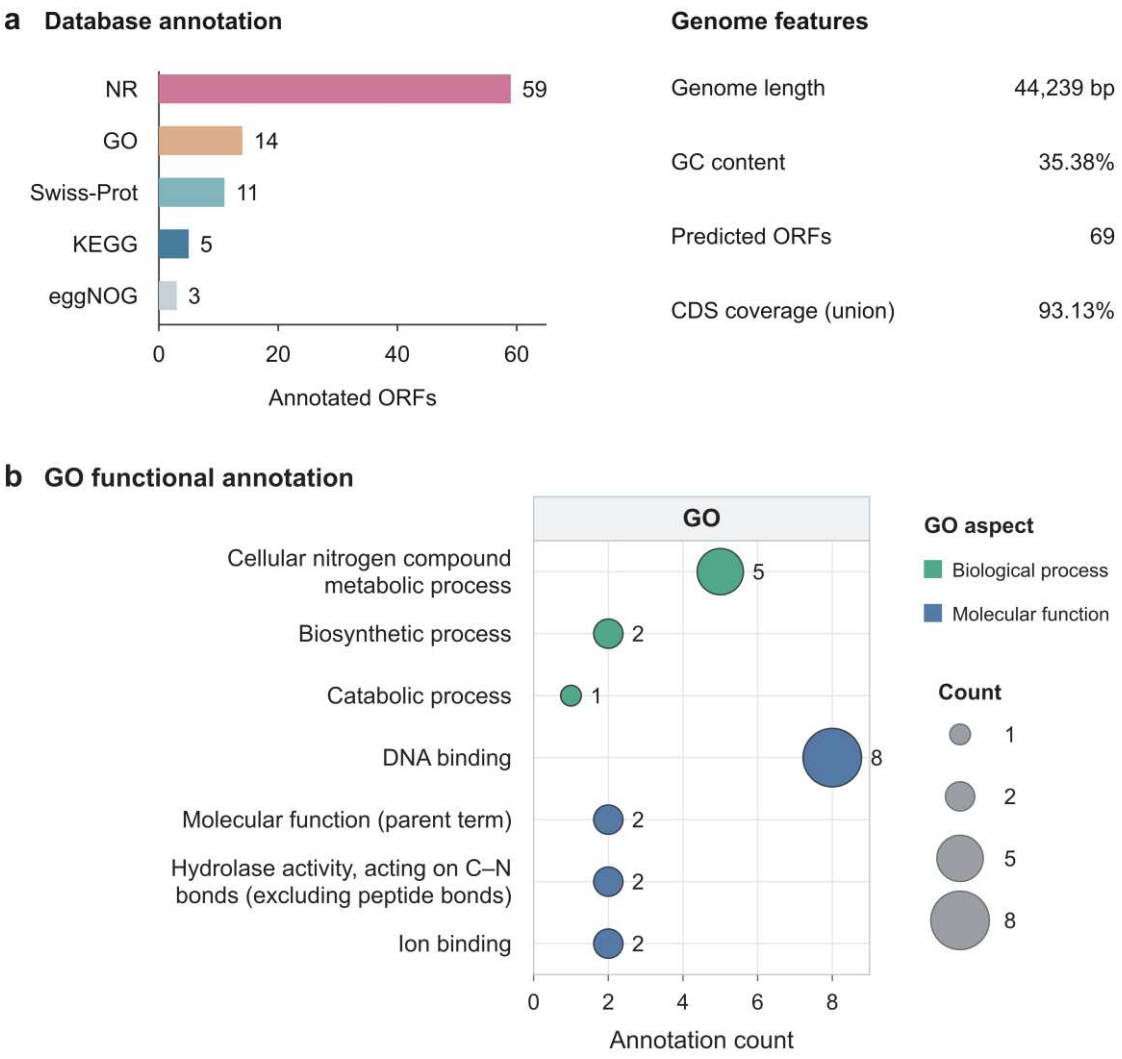


Figure 7. Genome features and functional annotations of phage SJP49-2.

(a) Database-annotated GeneMarkS CDSs and genome features; database hit sets may overlap. Coding coverage is the union of GeneMarkS CDS intervals divided by assembly length (93.13%). (b) GO functional annotation counts. Horizontal position and bubble area indicate annotation entry counts, with exact values labeled. Green: biological process; blue: molecular function. The generic molecular function parent term is retained as reported. A CDS may contribute to multiple categories. The GeneMarkS CDS set summarized here is distinct from the PhageScope set displayed in Figure 6.

In the KEGG bubble plot, assignments comprised protein families associated with genetic information processing (5 entries), replication and repair (3), xenobiotics

biodegradation and metabolism (1), nucleotide metabolism (1), unclassified metabolism (1), and unclassified genetic information processing (1) (Figure S2). These annotations highlight nucleic acid binding and genetic information processing within the annotated genome. Category counts can overlap because an ORF may have multiple assignments.

The product-based display groups in Figure 6 comprised two ORFs assigned to DNA packaging, 10 to virion structure or host interaction, five to DNA replication or metabolism, one to recombination, four to transcriptional regulation, 11 to other annotated functions or domains, and 36 to uncharacterized or uncertain functions. These mutually exclusive groups summarize specific product annotations; database coverage and GO/KEGG assignments were counted separately.

Packaging and structural/tail-related annotations were located within the first 18.93 kb of the assembled sequence, interspersed with ORFs assigned to other or uncertain functions. Representative annotations included a terminase-like protein (ORF02), portal protein (ORF03), capsid protein (ORF07), tail length tape measure protein (ORF16), and tail fiber protein (ORF21). The map also located candidate recombination and regulatory genes ORF28, ORF33, and ORF36; their annotation evidence is detailed in the section on lifestyle prediction and screening for safety-associated genes and Table S3. Independent inspection of the protein homology tables also identified an adjacent holin candidate (GeneMarkS SJP49_2_26; NR accession YP_009204279.1) and an endolysin candidate (GeneMarkS SJP49_2_27; YP_009045055.1), as well as a tail-associated cell-wall hydrolase candidate (GeneMarkS SJP49_2_24; YP_240843.1). These assignments are sequence-based predictions and do not establish enzymatic activity or the cause of the biofilm phenotype. Coordinate-specific annotation evidence is presented in Table S5 and Additional file 4.

Lifestyle Prediction and Screening for Safety-Associated Genes

PhageScope predicted a temperate lifestyle for SJP49-2. Functional annotation identified the candidate recombinase SJP49_2_28 (25,989–27,374 bp, reverse strand, 461 aa), transcriptional repressor SJP49_2_33 (30,131–30,346 bp, forward strand, 71 aa), and AntA/AntB antirepressor SJP49_2_36 (31,695–32,444 bp, forward strand, 249 aa). Their annotations implicate DNA recombination and transcriptional regulation and are consistent with the temperate lifestyle prediction. Candidate gene coordinates, protein product annotations, and annotation sources are listed in Table S3. In the NR results, the protein occupying the ORF28 coordinates matched an integrase (YP_010080142.1) at 95.01% identity across the 461-aa query, providing an independent homology-based line of support for recombination potential. GeneMarkS gene SJP49_2_37 corresponds by exact coordinates to PhageScope SJP49_2_36; these labels refer to the same antirepressor candidate.

The PhageScope screen returned no known virulence-factor or antimicrobial-resistance hits under the databases and settings used. This platform result was retained as a database-specific negative finding. Review of the NR table identified legacy product descriptions for SJP49_2_54 (NP_075488.1, labeled "Panton-Valentine leukocicin") and SJP49_2_55 (YP_010083859.1, labeled "virulence associated"). The corresponding PhageScope products were PVL ORF-50-like family and Phage Conserved Open Reading Frame 51, respectively. These inconsistent names do not establish functional leukocidin or virulence genes, but prevent an unqualified claim that all risk-associated functions have been excluded. Table S5 records the conflicting descriptions. SJP49_2_24 was annotated as a glycoside hydrolase in PhageScope and as a tail-associated cell-wall hydrolase in NR; neither annotation was treated as evidence for lysogeny-associated recombination.

Genomic Comparison of SJP49-2 with Reference Phages

The 19 reference phage genomes ranged from 41,392 to 44,221 bp, with GC contents of 34.56%–35.98%; all were assigned to *Phietavirus* in the downloaded GenBank records. Recorded countries of origin included Ireland, Italy, Argentina, the Czech Republic, France, the United States, Poland, China, and Turkey. Country information was unspecified for six reference phages. Reference names, accession numbers, and genome characteristics are provided in Table S2. The 44,239 bp genome of SJP49-2 was similar in length to those in the reference collection.

The circular comparison integrates the comparative tree for all 20 phages with country of origin, genome length, and GC content (Figure 8). SJP49-2 and DW2 (reference 1, Ireland) formed a terminal pair, with Sebago (reference 12, United States) on an adjacent branch; together with StauST398-3 (reference 10, France), they formed a smaller comparative group. The Argentine phages vB_SauS_760, vB_SauS_I73, vB_SauS_Mh1, and vB_SauS_287 occupied different branches, showing that clustering did not correspond directly to recorded country of origin in this collection. The GC content of SJP49-2 (35.38%) fell within the reference range, and its genome length of 44.24 kb was close to that of Rosita (44.22 kb).

A new local BLASTn comparison independently quantified sequence-level relationships within the same reference set. Query coverage, calculated from the union of reported aligned intervals, ranged from 63.68% to 76.75%. Hesat (OP947204.1) had the highest query coverage (76.75%); the highest-bit-score HSP for DW2 had 94.587% nucleotide identity over 10,253 aligned positions, with total query coverage of 72.74%. Thus, membership in the same displayed gene-content cluster did not imply genome-wide identity. HSP identities and coverage values are reported separately in Table S6 and Additional file 5; they were not treated as ANI, VIRIDIC similarity or a formal species assignment.

The gene presence–absence matrix (Figure 9) showed a set of conserved gene clusters shared by the 20 genomes, whereas the remaining clusters varied among phages. SJP49-2 retained a distinct combination of gene clusters relative to neighboring reference members, demonstrating its accessory gene composition against a shared genetic background.

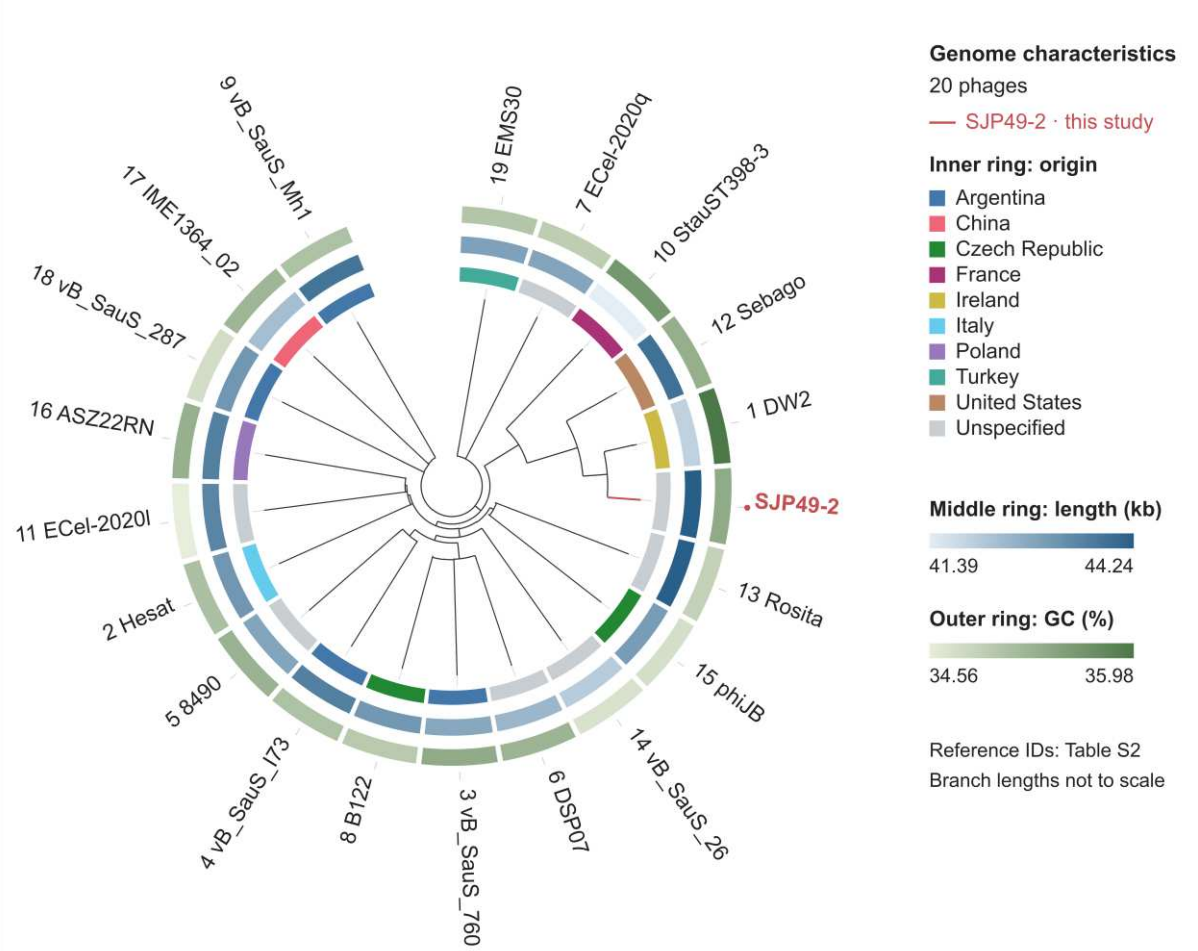


Figure 8. Comparative tree and genome characteristics of SJP49-2 and 19 reference phages.

SJP49-2 is highlighted in red. From inner to outer, the annotation rings show country of origin, genome length (kb), and GC content (%). Reference numbers correspond to Table S2. Gray origin sectors indicate unspecified country information. The circular layout displays the comparative clustering topology; branch lengths are not to scale. The gene presence–absence matrix is provided in Figure 9.

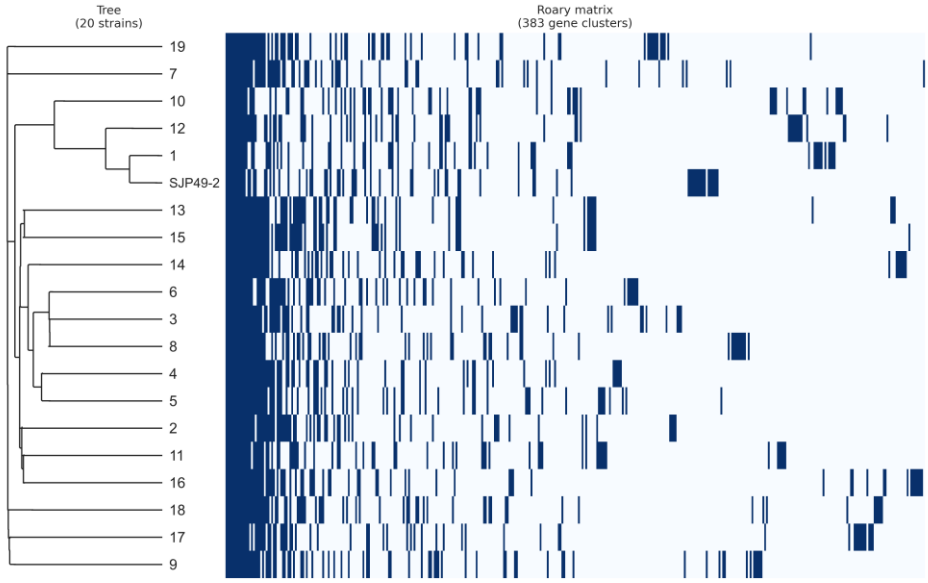


Figure 9. Comparative tree and gene presence–absence matrix of SJP49-2 and 19 reference phages.

Rows represent phage genomes, and columns represent gene clusters. Dark blue indicates presence; the pale background indicates absence from the detected gene clusters. The row labeled SJP49-2 represents the study phage (sequencing sample SJP49_2); numbers 1–19 correspond to the references in Table S2. The matrix contains 383 gene clusters. Tree tips are aligned, and branch lengths are not to scale.

Pangenome Composition of the Reference Collection

SJP49-2 and the 19 reference phages comprised 383 gene clusters (Figure 10). These included 11 core clusters (2.87%) present in all 20 genomes, one soft-core cluster (0.26%) present in 19 genomes, 133 shell clusters (34.73%) present in 3–18 genomes, and 238 cloud clusters (62.14%) present in 1–2 genomes. Core and soft-core clusters together comprised 12 high-frequency clusters, whereas shell and cloud clusters totaled 371 (96.87%). Using the strict core definition, 372 clusters (97.13%) were noncore. Thus, variable genes dominated

the pangenome of this collection, with low-frequency clusters contributing substantially to its gene diversity. These are descriptive counts for the supplied reference collection and gene-clustering result, rather than an estimate of a species-wide pangenome. Their interpretation is dependent on gene calling, reference selection and clustering settings.

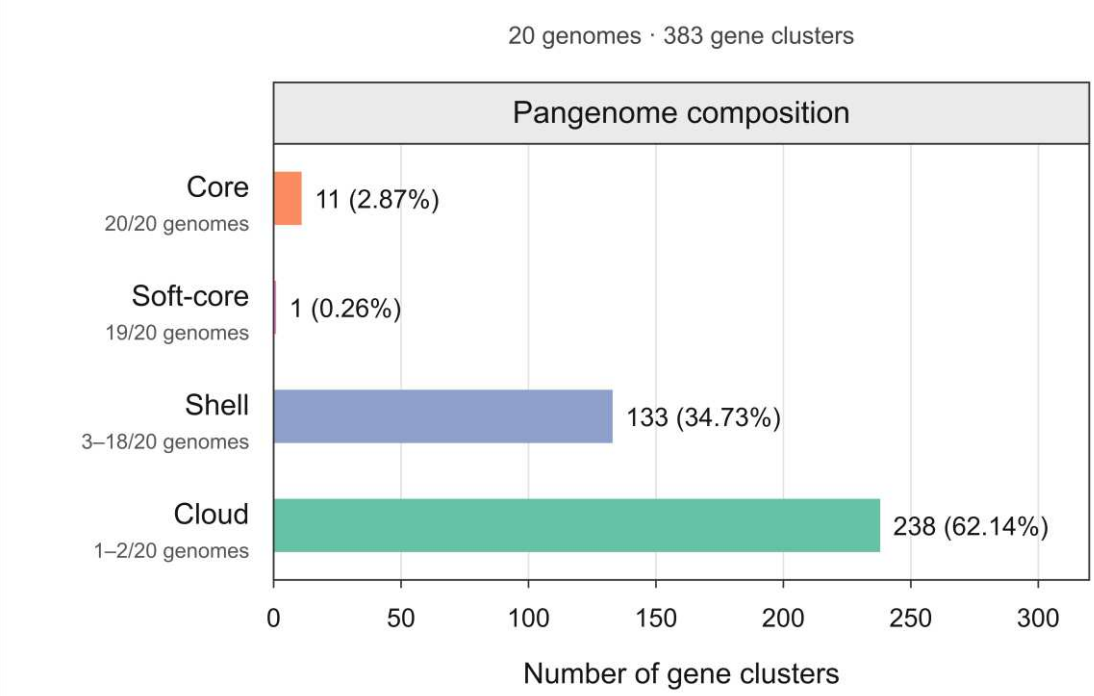


Figure 10. Pangenome composition of SJP49-2 and 19 reference phages. Counts and percentages are calculated from 383 gene clusters. Core, soft-core, shell, and cloud clusters occur in 20, 19, 3–18, and 1–2 of the 20 genomes, respectively.

Effects on Planktonic Growth of Host Strain P49-2

At 300 min, OD_{600} values at MOIs of 1000, 100, 10, 1, and 0.1 were 0.104, 0.120, 0.446, 0.619, and 0.732, respectively, compared with 1.307 for the control (Figure 11a). After correction against each group's 0 min value, all curves began at $\Delta OD_{600} = 0$ (Figure 11b).

At 300 min, ΔOD_{600} values at MOIs of 1000, 100, 10, 1, and 0.1 were −0.001, 0.010, 0.338, 0.517, and 0.659, respectively, compared with 1.249 for the control. Endpoint turbidity

in the MOI 1000 and 100 groups remained close to the corresponding starting levels, indicating strong inhibition of planktonic growth.

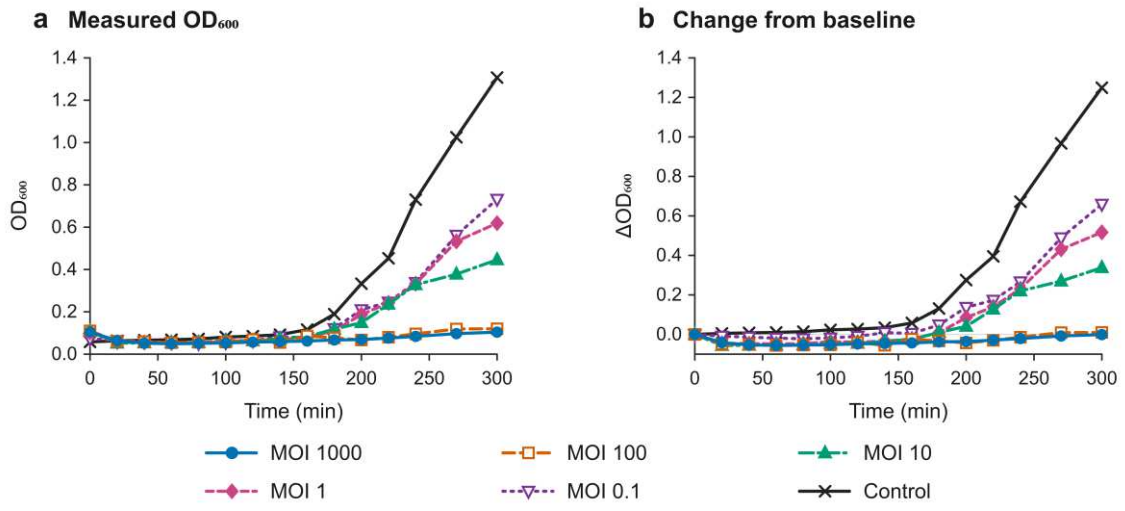


Figure 11. Planktonic growth of host strain P49-2 following phage SJP49-2 treatment. (a) Measured OD_{600}. (b) Changes relative to the 0 min value of each group: $\Delta OD_{600} = OD_{600}(t) - OD_{600}(0)$. Measured values and their corresponding baseline-adjusted values are shown at the selected sampling times.

Effects on Biofilm Formation

Crystal violet staining yielded mean $OD_{600} \pm$ SD values of 0.652 ± 0.053, 0.753 ± 0.155, 0.948 ± 0.112, and 1.220 ± 0.160 at MOIs of 1000, 100, 10, and 1, respectively, compared with 3.159 ± 0.203 for the control. Each group comprised five technical replicate readings within the same experiment (Figure 12a).

Based on group means, crystal violet signals in the four treatment groups were 79.36%, 76.16%, 69.98%, and 61.38% lower than the control, respectively. Attached biomass generally decreased as the MOI increased, supporting inhibition of biofilm formation by SJP49-2. The largest decrease occurred at an MOI of 1000.

Effects on Established Biofilms

Following treatment of established biofilms with phage titers of 10^8, 10^7, 10^6, and 10^5 PFU/mL, mean OD_{600} values calculated from four readings were 0.16175, 0.20400, 0.28000, and 0.35550, respectively, compared with 3.11275 for the control (Figure 12b). Residual crystal violet absorbance increased as the treatment titer decreased.

Using group means without blank subtraction, crystal violet signals in the four treatment groups were 94.80%, 93.45%, 91.00%, and 88.58% lower than the control, respectively. SJP49-2 reduced the attached biomass of established biofilms throughout the tested concentration range, with the largest reduction at 10^8 PFU/mL.

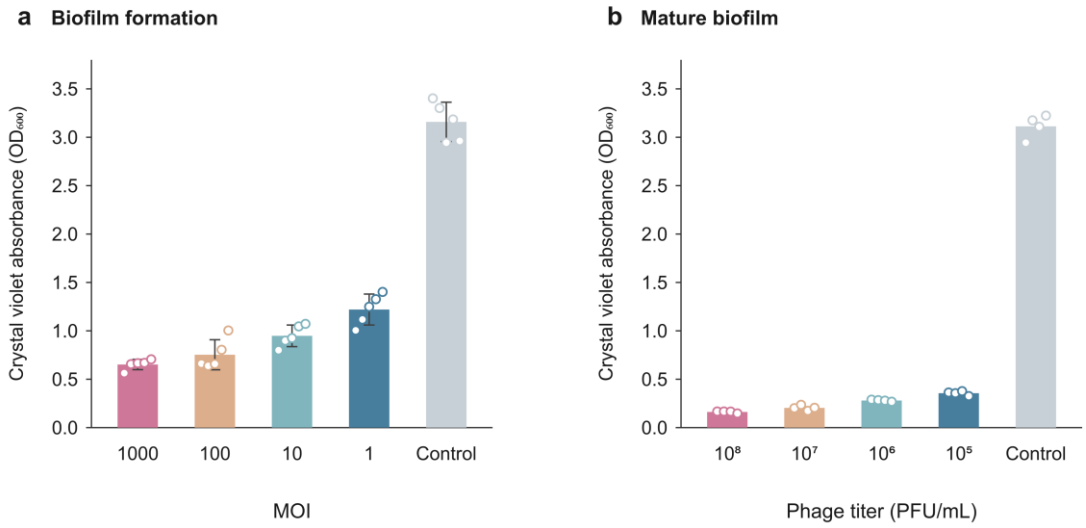
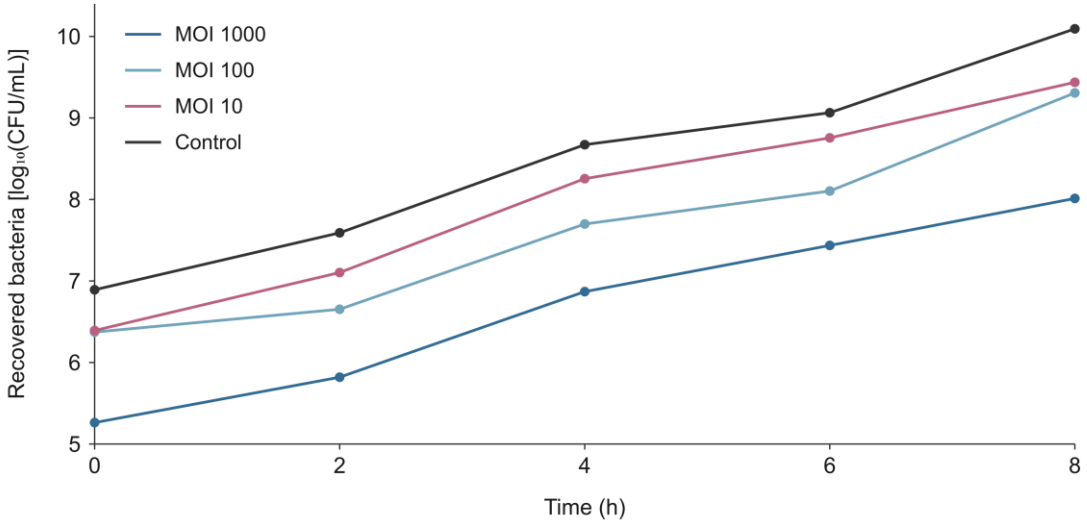


Figure 12. Effects of phage SJP49-2 on biofilms.

(a) Biofilm formation: bars show means, open circles show five technical replicate readings, and error bars show the SD among those readings. (b) Established biofilms: bars show means of four technical replicate readings, with individual readings shown as open circles. Each assay was performed once. Both assays measured crystal violet retention at 600 nm without blank subtraction.

Bacterial Counts in the Beef Surface Model

Different MOI inoculation schemes were established by adjusting both phage and bacterial inputs. Initial bacterial concentrations (CFU/mL) in the recovered filtrates from the MOI 1000, 100 and 10 groups and the phage-free control were 1.83×10^5, 2.36×10^6, 2.47×10^6 and 7.80×10^6, respectively. Counts increased in every group, reaching 1.03×10^8, 2.03×10^9, 2.74×10^9 and 1.24×10^{10} at 8 h. The corresponding endpoint differences from the control were 2.08, 0.79 and 0.66 $\log_{10}$ units. Increases from each group's own starting value were 2.75, 2.93, 3.05 and 3.20 $\log_{10}$ units, respectively. Thus, the phage-treated schemes had both lower endpoint counts and smaller observed rises than the control; the largest separation occurred in the MOI 1000 scheme, with a rise 0.45 $\log_{10}$ units smaller than the control (Figure 13).



634

635 **Figure 13. Recovered *Staphylococcus aureus* concentrations in the inoculated beef**

636 **model.**

637 Bacterial concentrations in recovered filtrates are plotted as $\log_{10}$(CFU/mL), with lines

638 connecting successive time points in a single experiment. Phage and bacterial inputs were

639 adjusted to establish the indicated initial MOIs, resulting in different starting bacterial counts.

640 Endpoint differences and changes from each group's measured 0 h value were reported

641 separately. These are descriptive comparisons of the tested inoculation schemes.

642 **Discussion**

643 **Host Coverage and Research Value of SJP49-2**

644 Plaque photographs and electron microscopy establish the morphological features of

645 SJP49-2 and complement its characterization in terms of plaque phenotype, virion structure,

646 lysis coverage, environmental stability, and propagation dynamics in culture. In their study of

647 *S. aureus* phage SA2, Wang et al. reported plaque morphology, head–tail structure, EOP, and

648 one-step growth parameters, which describe infection phenotypes, particle structure, and

649 productive infection, respectively [38]. The approximately isometric, polyhedral heads and

long, flexible tails of SJP49-2 are consistent with a siphovirus morphotype. Following the ICTV taxonomy update, siphovirus remains a morphological descriptor, whereas the abolished family *Siphoviridae* is no longer a formal taxonomic assignment. Classification of SJP49-2 should be based on genomic relationships [39].

SJP49-2 lysed 69.57% of the 92 tested *S. aureus* strains, exceeding the coverage of the other three candidates. This lysis coverage provides a direct basis for candidate selection, whereas EOP can further characterize propagation on different hosts [7]. Together, these measures can define the strains appropriate for SJP49-2 alone or in combination with other phages. Strain-specific EOP measurements quantify plaque formation by the same phage preparation across hosts and help distinguish a positive lysis phenotype from sustained productive infection. The 69.57% value reported here describes lysis coverage within the tested strain collection.

Genome-based identification supported the assignment of host strain P49-2 to *S. aureus* and provided information on adherence, biofilm-associated features, and phage-related genetic elements. Multistrain studies have linked phage susceptibility to host genetic background [6]. The host genome assembled here therefore provides a basis for investigating receptor recognition and defense mechanisms.

Environmental Tolerance and Phage Propagation

The endpoint titer of 8.75×10^8 PFU/mL at an MOI of 100 provides an initial condition for optimizing phage production. In planktonic assays, both MOI 1000 and 100 treatments maintained small net increases in turbidity. Related studies have likewise evaluated propagation conditions separately from inhibition of planktonic cells and biofilms [4]. Production conditions and application doses should therefore be optimized for their respective outcomes, taking the bacterial load and food matrix into account.

SJP49-2 retained relatively high residual titers after 1 h at pH 6–8, whereas titers were lower after treatment at 50 °C or above. This profile supports prioritizing studies of mild processing conditions and postprocessing contamination control. The reported inactivation of SPB at 70 °C [4] is consistent with the high-temperature sensitivity observed here. Low residual titers remained detectable for SJP49-2 at 80 °C, indicating differences in thermal tolerance among phages and treatment systems.

The propagation curve rose rapidly between 60 and 80 min, reached 9.77×10^8 PFU/mL at 80 min, and then declined. This pattern describes titer accumulation in the culture system used and can guide optimization of culture duration and harvest timing. Determination of the latent period and burst size would require a one-step growth experiment with synchronized adsorption and control of unadsorbed phages and infected-cell numbers [12]. Accordingly, 80 min is reported here as the time of peak culture titer, an operational indicator for selecting a harvest time.

Relationship between Planktonic and Biofilm Responses

SJP49-2 restricted the rise in planktonic turbidity and reduced biofilm-associated crystal violet retention. At 300 min, ΔOD_{600} values were −0.001 and 0.010 in the MOI 1000 and 100 groups, compared with 1.249 in the control. The highest-dose groups showed 79.36% lower staining during biofilm formation and 94.80% lower staining after treatment of established biofilms. These observations identify effects across suspended growth and two attachment-associated assay settings.

Crystal violet assays provide an established measure of retained attached biomass, while biofilm-cell metabolism or viable counts describe additional endpoints [32, 33]. The separation of formation and established-biofilm assays is also used in *S. aureus* phage studies such as the SPB investigation [4]. Accordingly, the present decreases support inhibition of

biomass accumulation and reduced retention of pre-established attached material. They do not by themselves quantify the fraction of biofilm cells killed or establish a specific matrix-degrading mechanism.

Control Performance in the Beef Model

The different starting counts in the beef model resulted from the chosen phage-to-host inoculation schemes. MOI is a ratio, and it can be changed by altering phage input, bacterial input or both; Hall et al. manipulated it through host-cell numbers [40], while Kim et al. examined bacterial inoculum size alongside the phage input ratio in a *S. aureus* propagation system [41]. These studies support describing the present design in terms of its input combinations. Their findings do not establish an equivalent treatment effect in the present food model. Abedon emphasized that absolute input quantities and exposure conditions also matter when interpreting MOI [34].

Within the tested schemes, all phage-treated groups had lower 8 h counts and smaller rises from their own starting values than the phage-free control. The MOI 1000 scheme showed the largest separation: its endpoint was 2.08 $\log_{10}$ units below the control, while its observed rise was 0.45 $\log_{10}$ units smaller. This pattern is consistent with growth limitation under that inoculation scheme. *S. aureus* phages have also shown activity in beef in the study by Gungor et al. [5], providing relevant food-matrix context. Here, the observed ranking concerns the complete input schemes: unequal starting loads prevent isolation of the contribution of phage treatment or MOI alone, and subtracting baseline growth does not remove that dependence. Bacterial counts rose in all groups, so the observation describes restricted accumulation relative to the control rather than elimination of the inoculum.

Genome Composition and Evaluation of Application Suitability

The draft genome of P49-2 was approximately 2.72 Mb, and the 44,239 bp assembled genome of SJP49-2 contained 69 predicted ORFs. Comparison with 19 complete *S. aureus* phage genomes defined the shared genetic background and accessory gene composition of SJP49-2. Kwan et al. identified an approximately 40 kb genome-size group in a comparison of 27 *S. aureus* phages [8]. An analysis of 205 staphylococcal phages by Oliveira et al. further showed extensive gene-content differences among genomes of similar sizes and demonstrated the value of shared protein families for describing genetic diversity [9]. Although reference genome lengths in the present collection were concentrated between 41.39 and 44.22 kb, the 20 genomes comprised 383 gene clusters. Similar genome lengths thus did not imply identical gene content.

The annotated map adds positional context to these comparisons. The concentration of packaging and structural/tail-related annotations within the first 18.93 kb of SJP49-2 is consistent with the functional gene organization described for staphylococcal phages [42]. Terminase-like, portal, capsid, tape measure, and tail fiber annotations identify candidates for investigating DNA packaging, particle assembly, and host interaction. Their genomic positions and predicted products provide a basis for targeted experiments, but do not establish coordinated expression, receptor specificity, or the mechanism underlying the observed lysis coverage. The 36 ORFs with uncharacterized or uncertain functions also limit a complete mechanistic interpretation.

The NR results assigned SJP49_2_24 to a tail-associated cell-wall hydrolase and SJP49_2_27 to a DW2-related endolysin, while Swiss-Prot supported hydrolase/autolysin homology for both. This agreement across annotation sources identifies candidates for future biochemical study. Keary et al. demonstrated antibacterial functions of the DW2 endolysin and tail hydrolase [10], but activity of a homolog cannot establish the substrate specificity or

activity of the SJP49-2 proteins. No purified-protein assay was performed here, so the whole-phage biofilm phenotype cannot be attributed to either candidate. Conservative assignment of protein functions and separation of structural from functional annotation follow phage annotation guidance [25]. The GC-content and GC-skew tracks describe local sequence composition and do not establish a replication origin, lysogeny or a circular physical genome.

GO describes gene products in terms of biological process, molecular function, and cellular component; its hierarchical structure permits multiple terms to be associated with a protein [21]. KEGG maps gene products through orthologous functions to pathways and BRITE hierarchies, providing a complementary description of genome function [23]. DNA binding was the most represented GO category in SJP49-2, whereas protein families related to genetic information processing and replication and repair predominated among its KEGG assignments. These complementary annotations identify nucleic acid-related functions as an important component of the annotated genome and provide a defined direction for selecting candidate proteins involved in genome replication and nucleic acid regulation. Hydrolase activity acting on carbon–nitrogen bonds, ion binding, and nucleotide metabolism further describe candidate catalytic and binding functions.

The bubble plots display category names, annotation counts, and functional classifications for direct comparison. The GO molecular function parent term is retained as a hierarchical assignment and is not interpreted as a specific molecular activity. KEGG pathway categories and BRITE protein family categories retain their respective meanings. Because categories overlap, assignment to a pathway category does not establish that all components of that pathway have been identified. These counts describe genomic functional annotations rather than expression changes or statistically significant enrichment [21, 23].

The collection contained only 11 strict core clusters, together with 133 shell and 238 cloud clusters, indicating a small shared core and extensive variable gene content. This

770 composition agrees with the alternating conserved and variable patterns in the gene presence–
771 absence matrix. Kwan et al. documented extensive genomic mosaicism among *S. aureus*
772 phages, and Oliveira et al. found homologous genes in different genomic backgrounds [8, 9].
773 Across 188 *S. aureus* phages, Zhou et al. identified conserved morphogenesis and DNA-
774 packaging clusters alongside other functional modules with varying degrees of divergence
775 [42]. These studies show how conserved modules and variable gene combinations jointly
776 shape staphylococcal phage diversity. The distribution observed here follows this pattern and
777 highlights the contribution of accessory gene composition to differences among the reference
778 phages. Roary was developed for prokaryotic pangenome analysis using annotated genomes
779 from the same species [28]. Application to this phage reference collection therefore requires
780 caution: variable gene counts can reflect divergence and differences in gene predictions as
781 well as biological accessory genes. The comparative result is reported without interpreting its
782 small core as proof of an open pangenome or as sufficient evidence for a new species. The
783 new BLASTn coverage analysis provides a separately reproducible description of nucleotide-
784 level relatedness.

785 SJP49-2 and DW2 formed a terminal pair in the comparative tree, yet their gene
786 compositions remained distinguishable in the presence–absence matrix. The circular
787 annotations also showed that references with similar genome lengths and GC contents
788 occurred on different branches, and the four Argentine phages did not form a single branch.
789 Country of origin and overall genome composition therefore did not fully capture gene-
790 cluster differences in this collection. SJP49-2 combines a genetic background shared with
791 neighboring references and a distinct accessory gene repertoire. This comparison provides
792 context for relating its antibacterial phenotype to candidate host-recognition, infection, and
793 antimicrobial functions. Shared gene-cluster patterns describe relationships within the

reference collection; viral classification remains subject to the ICTV sequence-based framework [39].

A temperate lifestyle prediction is compatible with the antibacterial phenotypes observed here. The candidate recombinase (ORF28), transcriptional repressor (ORF33), and AntA/AntB antirepressor (ORF36), localized in Figure 6 and documented in Table S3, are consistent with recombination and regulatory features reported in temperate staphylococcal phages. Keary et al. identified recombinase, repressor, and antirepressor genes in temperate phage DW2 and demonstrated lytic activity against growing hosts [10]. The lysis coverage, planktonic growth inhibition, and biofilm findings therefore support antibacterial activity of SJP49-2, while its lifestyle interpretation rests on computational prediction and candidate functional gene annotations.

The lifestyle interpretation remains a genome-supported temperate prediction. In *S. aureus* phages, Thabet et al. experimentally established CI-repressor function and prophage induction [43]; the SJP49-2 repressor annotation alone does not provide equivalent functional confirmation. This distinction preserves the antibacterial observations while defining the scope of the lifestyle inference.

The negative PhageScope result should be interpreted alongside the inconsistent product labels recovered from the functional annotation. PVL is a bicomponent toxin encoded by lukS-PV and lukF-PV; the characterization of PVL-converting phage phiSLT established these specific toxin genes and their biological effects [26]. An ORF-50-like family label or a generic "virulence associated" description is insufficient to assign that toxin function. Conversely, conflicting annotations cannot be dismissed merely because one database screen returned no hits. The present study therefore does not establish absence of all virulence-associated functions or application safety. Gene-specific curation against validated reference proteins and explicit screening provenance remain necessary. Host DNA transfer is a separate

819 issue: Chen et al. demonstrated lateral transduction in some temperate *S. aureus* phages [44],
820 but the present study did not test or demonstrate transduction by SJP49-2. Taken together,
821 SJP49-2 is treated as a phage biology resource with observed antibacterial and biofilm-
822 biomass phenotypes.

823 This interpretation defines practical development priorities: assessment of lysogeny and
824 gene transfer, characterization of key antibacterial proteins, and comparison with strictly lytic
825 phages. Functional studies of the DW2 endolysin and tail hydrolase show that temperate
826 phages can also provide antibacterial enzyme resources [10]. The candidate proteins and
827 antibiofilm responses of SJP49-2 therefore provide specific starting points for studies of
828 infection mechanisms and antimicrobial components.

829 The phenotypic results describe single experiments with technical replication, which
830 characterizes within-experiment variation but does not establish between-experiment
831 reproducibility [36]. Crystal violet retention measures attached biomass, and the beef
832 comparison incorporates unequal starting loads associated with its input schemes. These
833 features limit inference about cell killing, isolated treatment effects and generalizability.
834 Genomic evidence is likewise interpreted within the available annotation and assembly
835 records; gap-free sequence alone does not verify virion DNA topology or application safety
836 [25].

837 **Conclusions**

838 SJP49-2 showed lysis against 64 of 92 laboratory-maintained *S. aureus* strains, restricted
839 planktonic turbidity increases and reduced crystal violet retention during biofilm formation
840 and after treatment of established biofilms. In the beef experiment, phage-containing
841 inoculation schemes showed lower endpoint bacterial counts and smaller observed increases
842 than the control, with the largest separation at MOI 1000. The 44,239 bp assembly, gene

annotations and reference comparisons add genomic context to these phenotypes. Together, the findings support SJP49-2 as a resource for phage–host and food-related biocontrol research, with the scope of the phenotypic and genomic inferences defined by the study design.

Declarations

Ethics approval and consent to participate

This study used bacterial strains and bacteriophages from slaughter and processing samples and did not involve human participants or experimental procedures on live animals.

Consent for publication

Not applicable.

Availability of data and materials

The draft genome of *Staphylococcus aureus* P49-2 has been deposited in DDBJ/ENA/GenBank under accession JCFQZX000000000; the version described here is JCFQZX010000000 (BioProject PRJNA1549128; BioSample SAMN64377570). The phage assembly is associated with GenBank accession QB220577. Supplementary tables and figures, sequencing statistics, software settings, gene annotations and BLASTn comparisons are included in Additional files 1–5. Analysis scripts, input sequences and BLASTn alignment output are provided in Additional file 6.

Competing interests

The authors declare that they have no competing interests.

Funding

This research was funded by the Science and Technology Program of the Xinjiang Uyghur Autonomous Region (Key Research and Development Program), grant number 2026B02002.

Authors' contributions

B.P. and Q.H. conceptualized the study. Q.H. and J.Q. developed the methodology. Q.H., J.Q. and X.H. performed the investigation. Q.H. and X.H. conducted the formal analysis. Q.H. curated the data and wrote the original draft. B.P., J.Q. and X.H. reviewed and edited the manuscript. B.P. supervised the study. All authors read and approved the final manuscript.

Acknowledgements

The authors would like to thank the College of Veterinary Medicine, Xinjiang Agricultural University, and the Xinjiang Regional Key Laboratory of Clinical Veterinary Medicine Research for providing laboratory facilities and technical support for this study.

References

1. Asao T, Kumeda Y, Kawai T, Shibata T, Oda H, Haruki K, et al. An extensive outbreak of staphylococcal food poisoning due to low-fat milk in Japan: estimation of enterotoxin A in the incriminated milk and powdered skim milk. Epidemiol Infect. 2003;130:33-40. https://doi.org/10.1017/S0950268802007951.

2. Waters AE, Contente-Cuomo T, Buchhagen J, Liu CM, Watson L, Pearce K, et al. Multidrug-Resistant *Staphylococcus aureus* in US Meat and Poultry. Clin Infect Dis. 2011;52:1227-1230. https://doi.org/10.1093/cid/cir181.

884 3. de Souza EL, Meira QGS, de Medeiros Barbosa I, Athayde AJAA, da Conceição ML, de
885 Siqueira Júnior JP. Biofilm formation by *Staphylococcus aureus* from food contact surfaces
886 in a meat-based broth and sensitivity to sanitizers. Braz J Microbiol. 2014;45:67-75.
887 https://doi.org/10.1590/S1517-83822014000100010.
888 4. Ma L, Liu Y, Zheng X, Zheng B, Cheng Y, Cai Y, et al. Isolation and characterization of
889 methicillin-resistant *Staphylococcus aureus* phage SPB against MRSA planktonic cells and
890 biofilm. Front Microbiol. 2025;16:1554182. https://doi.org/10.3389/fmicb.2025.1554182.
891 5. Gungor C, Onmaz NE, Gundog DA, Yavas GT, Koskeroglu K, Gungor G. Four novel
892 bacteriophages from slaughterhouse: Their potency on control of biofilm-forming MDR *S.*
893 *aureus* in beef model. Food Control. 2024;156:110146.
894 https://doi.org/10.1016/j.foodcont.2023.110146.
895 6. Moller AG, Winston K, Ji S, Wang J, Hargita Davis MN, Solís-Lemus CR, et al. Genes
896 Influencing Phage Host Range in *Staphylococcus aureus* on a Species-Wide Scale. mSphere.
897 2021;6:e01263-20. https://doi.org/10.1128/mSphere.01263-20.
898 7. Khan Mirzaei M, Nilsson AS. Isolation of Phages for Phage Therapy: A Comparison of
899 Spot Tests and Efficiency of Plating Analyses for Determination of Host Range and Efficacy.
900 PLoS One. 2015;10:e0118557. https://doi.org/10.1371/journal.pone.0118557.
901 8. Kwan T, Liu J, DuBow M, Gros P, Pelletier J. The complete genomes and proteomes of 27
902 *Staphylococcus aureus* bacteriophages. Proc Natl Acad Sci U S A. 2005;102:5174-5179.
903 https://doi.org/10.1073/pnas.0501140102.
904 9. Oliveira H, Sampaio M, Melo LDR, Dias O, Pope WH, Hatfull GF, et al. Staphylococci
905 phages display vast genomic diversity and evolutionary relationships. BMC Genomics.
906 2019;20:357. https://doi.org/10.1186/s12864-019-5647-8.

907 10. Keary R, McAuliffe O, Ross RP, Hill C, O'Mahony J, Coffey A. Genome analysis of the
908 staphylococcal temperate phage DW2 and functional studies on the endolysin and tail
909 hydrolase. Bacteriophage. 2014;4:e28451. https://doi.org/10.4161/bact.28451.
910 11. Kropinski AM, Mazzocco A, Waddell TE, Lingohr E, Johnson RP. Enumeration of
911 bacteriophages by double agar overlay plaque assay. Methods Mol Biol. 2009;501:69-76.
912 https://doi.org/10.1007/978-1-60327-164-6_7.
913 12. Hyman P, Abedon ST. Practical methods for determining phage growth parameters.
914 Methods Mol Biol. 2009;501:175-202. https://doi.org/10.1007/978-1-60327-164-6_18.
915 13. Chen S, Zhou Y, Chen Y, Gu J. fastp: an ultra-fast all-in-one FASTQ preprocessor.
916 Bioinformatics. 2018;34:i884-i890. https://doi.org/10.1093/bioinformatics/bty560.
917 14. Bankevich A, Nurk S, Antipov D, Gurevich AA, Dvorkin M, Kulikov AS, et al. SPAdes:
918 a new genome assembly algorithm and its applications to single-cell sequencing. J Comput
919 Biol. 2012;19:455-477. https://doi.org/10.1089/cmb.2012.0021.
920 15. Walker BJ, Abeel T, Shea T, Priest M, Abouelliel A, Sakthikumar S, et al. Pilon: an
921 integrated tool for comprehensive microbial variant detection and genome assembly
922 improvement. PLoS One. 2014;9:e112963. https://doi.org/10.1371/journal.pone.0112963.
923 16. Parks DH, Imelfort M, Skennerton CT, Hugenholtz P, Tyson GW. CheckM: assessing the
924 quality of microbial genomes recovered from isolates, single cells, and metagenomes.
925 Genome Res. 2015;25:1043-1055. https://doi.org/10.1101/gr.186072.114.
926 17. Chaumeil PA, Mussig AJ, Hugenholtz P, Parks DH. GTDB-Tk: a toolkit to classify
927 genomes with the Genome Taxonomy Database. Bioinformatics. 2020;36:1925-1927.
928 https://doi.org/10.1093/bioinformatics/btz848.

18. Besemer J, Lomsadze A, Borodovsky M. GeneMarkS: a self-training method for prediction of gene starts in microbial genomes. Implications for finding sequence motifs in regulatory regions. Nucleic Acids Res. 2001;29:2607-2618. https://doi.org/10.1093/nar/29.12.2607.

19. Kalvari I, Nawrocki EP, Ontiveros-Palacios N, Argasinska J, Lamkiewicz K, Marz M, et al. Rfam 14: expanded coverage of metagenomic, viral and microRNA families. Nucleic Acids Res. 2021;49:D192-D200. https://doi.org/10.1093/nar/gkaa1047.

20. Buchfink B, Xie C, Huson DH. Fast and sensitive protein alignment using DIAMOND. Nat Methods. 2015;12:59-60. https://doi.org/10.1038/nmeth.3176.

21. The Gene Ontology Consortium. The Gene Ontology knowledgebase in 2023. Genetics. 2023;224:iyad031. https://doi.org/10.1093/genetics/iyad031.

22. Jones P, Binns D, Chang HY, Fraser M, Li W, McAnulla C, et al. InterProScan 5: genome-scale protein function classification. Bioinformatics. 2014;30:1236-1240. https://doi.org/10.1093/bioinformatics/btu031.

23. Kanehisa M, Furumichi M, Sato Y, Kawashima M, Ishiguro-Watanabe M. KEGG for taxonomy-based analysis of pathways and genomes. Nucleic Acids Res. 2023;51:D587-D592. https://doi.org/10.1093/nar/gkac963.

24. Wang RH, Yang S, Liu Z, Zhang Y, Wang X, Xu Z, et al. PhageScope: a well-annotated bacteriophage database with automatic analyses and visualizations. Nucleic Acids Res. 2024;52:D756-D761. https://doi.org/10.1093/nar/gkad979.

25. Turner D, Adriaenssens EM, Tolstoy I, Kropinski AM. Phage Annotation Guide: Guidelines for Assembly and High-Quality Annotation. PHAGE. 2021;2:170-182. https://doi.org/10.1089/phage.2021.0013.

26. Narita S, Kaneko J, Chiba J, Piemont Y, Jarraud S, Etienne J, et al. Phage conversion of Panton-Valentine leukocidin in *Staphylococcus aureus*: molecular analysis of a PVL-

954 converting phage, phiSLT. Gene. 2001;268:195-206. https://doi.org/10.1016/S0378-
955 1119(01)00390-0.
956 27. Seemann T. Prokka: rapid prokaryotic genome annotation. Bioinformatics. 2014;30:2068-
957 2069. https://doi.org/10.1093/bioinformatics/btu153.
958 28. Page AJ, Cummins CA, Hunt M, Wong VK, Reuter S, Holden MTG, et al. Roary: rapid
959 large-scale prokaryote pan genome analysis. Bioinformatics. 2015;31:3691-3693.
960 https://doi.org/10.1093/bioinformatics/btv421.
961 29. Xu S, Dai Z, Guo P, Fu X, Liu S, Zhou L, et al. ggtreeExtra: Compact Visualization of
962 Richly Annotated Phylogenetic Data. Mol Biol Evol. 2021;38:4039-4042.
963 https://doi.org/10.1093/molbev/msab166.
964 30. Camacho C, Coulouris G, Avagyan V, Ma N, Papadopoulos J, Bealer K, et al. BLAST+:
965 architecture and applications. BMC Bioinformatics. 2009;10:421.
966 https://doi.org/10.1186/1471-2105-10-421.
967 31. Workman RE, Stoltzfus MJ, Keith NC, Euler CW, Bondy-Denomy J, Modell JW. Anti-
968 CRISPR proteins trigger a burst of CRISPR-Cas9 expression that enhances phage defense.
969 Cell Rep. 2024;43:113849. https://doi.org/10.1016/j.celrep.2024.113849.
970 32. O'Toole GA. Microtiter dish biofilm formation assay. J Vis Exp. 2011;47:2437.
971 https://doi.org/10.3791/2437.
972 33. Haney EF, Trimble MJ, Hancock REW. Microtiter plate assays to assess antibiofilm
973 activity against bacteria. Nat Protoc. 2021;16:2615-2632. https://doi.org/10.1038/s41596-
974 021-00515-3.
975 34. Abedon ST. Phage therapy dosing: The problem(s) with multiplicity of infection (MOI).
976 Bacteriophage. 2016;6:e1220348. https://doi.org/10.1080/21597081.2016.1220348.
977 35. Sanders ER. Aseptic laboratory techniques: plating methods. J Vis Exp. 2012;(63):e3064.
978 https://doi.org/10.3791/3064.

979 36. Lazic SE, Clarke-Williams CJ, Munafò MR. What exactly is “N” in cell culture and
980 animal experiments? PLoS Biol. 2018;16:e2005282.
981 https://doi.org/10.1371/journal.pbio.2005282.
982 37. Lang TA, Altman DG. Basic statistical reporting for articles published in biomedical
983 journals: the Statistical Analyses and Methods in the Published Literature or the SAMPL
984 Guidelines. Int J Nurs Stud. 2015;52:5-9. https://doi.org/10.1016/j.ijnurstu.2014.09.006.
985 38. Wang J, Zhao F, Sun H, Wang Q, Zhang C, Liu W, et al. Isolation and characterization of
986 the *Staphylococcus aureus* bacteriophage vB_SauS_SA2. AIMS Microbiol. 2019;5:285-307.
987 https://doi.org/10.3934/microbiol.2019.3.285.
988 39. Turner D, Shkoporov AN, Lood C, Millard AD, Dutilh BE, Alfenas-Zerbini P, et al.
989 Abolishment of morphology-based taxa and change to binomial species names: 2022
990 taxonomy update of the ICTV bacterial viruses subcommittee. Arch Virol. 2023;168:74.
991 https://doi.org/10.1007/s00705-022-05694-2.
992 40. Hall AR, Scanlan PD, Leggett HC, Buckling A. Multiplicity of infection does not
993 accelerate infectivity evolution of viral parasites in laboratory microcosms. J Evol Biol.
994 2012;25:409-415. https://doi.org/10.1111/j.1420-9101.2011.02434.x.
995 41. Kim SG, Kwon J, Giri SS, Yun S, Kim HJ, Kim SW, et al. Strategy for mass production
996 of lytic *Staphylococcus aureus* bacteriophage pSa-3: contribution of multiplicity of infection
997 and response surface methodology. Microb Cell Fact. 2021;20:56.
998 https://doi.org/10.1186/s12934-021-01549-8.
999 42. Zhou W, Wen H, Li Y, Gao Y, Zheng X, Yuan L, et al. Whole-Genome Analysis Reveals
1000 That Bacteriophages Promote Environmental Adaptation of *Staphylococcus aureus* via Gene
1001 Exchange, Acquisition, and Loss. Viruses. 2022;14:1199. https://doi.org/10.3390/v14061199.

43. Thabet MA, Penadés JR, Haag AF. The ClpX protease is essential for inactivating the CI master repressor and completing prophage induction in *Staphylococcus aureus*. Nat Commun. 2023;14:6599. https://doi.org/10.1038/s41467-023-42413-0.

44. Chen J, Quiles-Puchalt N, Chiang YN, Bacigalupe R, Fillol-Salom A, Chee MSJ, et al. Genome hypermobility by lateral transduction. Science. 2018;362:207-212. https://doi.org/10.1126/science.aat5867.

Additional files

Additional file 1

File name: Additional_file_1_Supplementary_Tables_and_Figures.docx

File format: .docx

Title: Supplementary tables and figures

Description: Tables S1–S6 and Figures S1–S2 describing sequencing, reference phages, lifestyle-associated annotations, software settings and comparative analyses.

Additional file 2

File name: Additional_file_2_FASTQ_Statistics.csv

File format: .csv

Title: Sequencing read statistics

Description: Per-file raw and filtered read counts, nucleotide totals and sequence-length summaries for phage SJP49-2.

Additional file 3

File name: Additional_file_3_Software_and_Analysis_Settings.csv

File format: .csv

Title: Software and analysis settings

Description: Software versions and analysis settings corresponding to Table S4.

Additional file 4

File name: Additional_file_4_Gene_Annotations.csv

File format: .csv

Title: Gene annotations and coordinate correspondence

Description: GeneMarkS CDS coordinates, protein alignments and exact-coordinate correspondence with PhageScope predictions.

Additional file 5

File name: Additional_file_5_BLASTn_Comparison.csv

File format: .csv

Title: BLASTn comparison with reference genomes

Description: Union-based query and subject coverage, HSP counts and highest-bit-score HSP statistics for the 19 references.

Additional file 6

File name: Additional_file_6_Analysis_Resources.zip

File format: .zip

Title: Sequences and reproducible analysis resources

Description: Phage sequence and annotation files, reference sequences, BLASTn alignments, command parameters and scripts for recalculating summary statistics.

Supplementary Files

This is a list of supplementary files associated with this preprint. Click to download.

- Additionalfile2FASTQStatistics.csv
- Additionalfile5BLASTnComparison.csv
- Additionalfile6AnalysisResources.zip
- Additionalfile1SupplementaryTablesandFigures.docx
- Additionalfile3SoftwareandAnalysisSettings.csv